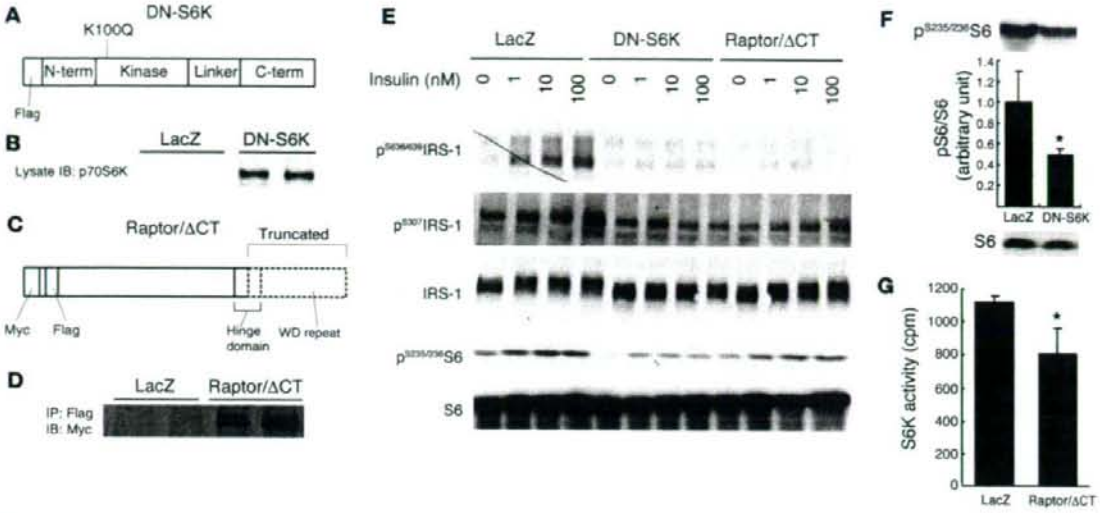

Figure 8

Hypothalamic overexpression of DN-S6K or Raptor/ΔCT and functional validation of these viruses in hypothalamic GT1-7 cells and rat MBH. (**A**) Construction of kinase-dead DN-S6K. (**B**) Confirmation of DN-S6K expression in the MBH. (**C**) Construction of Raptor/ΔCT. A part of the hinge domain and all WD repeat domains were removed. The N terminus had Myc and Flag tags. (**D**) Confirmation of Raptor/ΔCT expression in the MBH. MBH lysate was immunoprecipitated with anti-Flag antibody and immunoblotted with anti-Myc antibody. (**E**) Adenovirus-infected GT1-7 cells were stimulated with 0, 1, 10, or 100 nM insulin for 30 min. Serine phosphorylations in the insulin-stimulated state of S6 and IRS-1 at Ser636/639 and Ser307 were significantly reduced by DN-S6K and Raptor/ΔCT overexpression (phosphoproteins/total protein ratio, $P < 0.01$, 2-way repeated-measures ANOVA; $n = 2$). Representative bands are shown. (**F**) Overexpression of DN-S6K suppressed phosphorylation of S6 in the MBH of rats fed HFD for 1 d. (**G**) Overexpression of Raptor/ΔCT suppressed S6K activity in the MBH of 1 d HFD-fed rats. *$P < 0.05$ versus LacZ.

Discussion

Here we demonstrate, for the first time to our knowledge, that a single day of exposure to a HFD blunts both insulin signaling in the hypothalamus and the ability of hypothalamic insulin to suppress HGP. This blunting is accompanied by activation of S6K, suggesting a role for this molecule in the mediation of central insulin sensitivity and peripheral glucose homeostasis. To investigate the role of hypothalamic S6K in short-term HFD–induced hepatic insulin resistance, we expressed gain- and loss-of-function mutants of the mTOR/S6K pathway selectively in the MBH using targeted adenovirus injections. MBH overexpression of CA-S6K mimicked the hypothalamic metabolic and signaling consequences of 1-d HFD feeding, characterized by blunted insulin sensitivity during a pancreatic basal clamp with MBH insulin and reduced hypothalamic insulin signaling. Overactivation of MBH S6K also induced hepatic insulin resistance under hyperinsulinemic clamp conditions. On the other hand, MBH overexpression of DN-S6K or Raptor/ΔCT in animals fed HFD for 1 d completely reversed diet-induced hypothalamic insulin insensitivity and signaling. These findings, together with the previous observations that short-term HFD induces hepatic insulin resistance and that the brain partly mediates the effect of insulin to suppress HGP (14–18), strongly suggest that the activation of hypothalamic mTOR/S6K induces the early onset of hepatic insulin resistance during HFD feeding in rodents.

Insulin sensitivity is tightly linked to nutrient availability in multiple systems. The development of insulin resistance in different tissues may be both temporally and mechanistically distinct. Although hypothalamic insulin resistance appears to be an early event in the development of HFD-induced hepatic insulin resistance, it is noteworthy that with more prolonged exposure to nutrient excess, alterations in insulin signaling have been documented in several peripheral tissues, including the liver, and that insulin resistance extends well beyond this brain-liver circuit. We and others have previously shown that more prolonged overfeeding (~7 d) is necessary to induce insulin resistance in peripheral tissues other than the liver (19, 20, 33). Changes in hepatic insulin signaling accompanying the development of insulin resistance also depend on the duration of nutrient excess. HFD or Western diet feeding for 10–14 d (34, 35) induces paradoxical enhancement of IRS signaling in the liver, while longer overfeeding induces inhibition (35). Based on our present data, we suggest that altered hypothalamic insulin signaling determines insulin resistance early during HFD feeding, while blunted hepatic insulin signaling substantially contributes to insulin resistance during more prolonged overnutrition.

Even in the hypothalamus, the duration of HFD feeding appears to induce different modification patterns of insulin signaling. The 1-d HFD-fed rat model displayed decreased activation of hypothalamic IRS-1 and Akt, in parallel with increased S6K activation, in the absence of any change in IR and IRS-2 tyrosine phosphorylation, JNK phosphorylation, or PTP-1B expression. S6K phosphorylation has also previously been shown to be elevated in the liver and muscle after 5 d of hyperinsulinemia (36) as well as in muscle and fat after 4 mo of HFD feeding (13); these studies did not assess S6K phosphorylation in the hypothalamus. Previously, 10–30 d of exposure to a Western diet has been shown to blunt

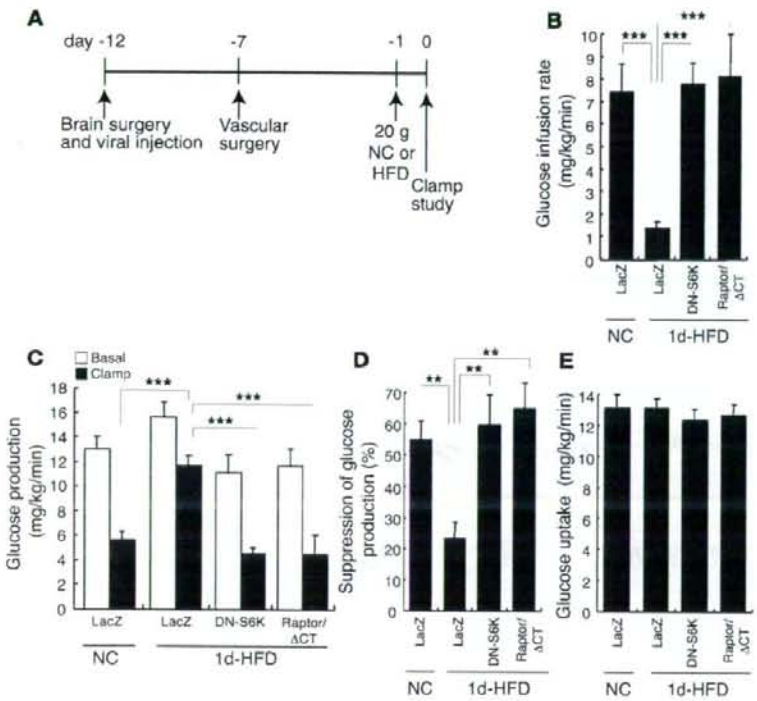

Figure 9

Hypothalamic overexpression of DN-S6K or Raptor/ΔCT reverses insulin resistance in HFD-fed rats. (**A**) DN-S6K or Raptor/ΔCT adenoviruses were injected into the MBH, and 12 d later, insulin clamp studies were performed on rats fed NC or HFD for 1 d. (**B**) Glucose infusion rate required to maintain euglycemia during the clamp period. (**C**) Glucose production during basal and clamp periods. (**D**) Clamp/basal HGP suppression ratio. (**E**) Peripheral glucose uptake during the clamp period. $^{**}P < 0.01$; $^{***}P < 0.001$.

tyrosine phosphorylation of IR, IRS-1, and IRS-2 as well as Akt phosphorylation in the hypothalamus, while JNK phosphorylation is increased (35). Moreover, PTP-1B was recently reported to be increased in the arcuate nucleus by 20 wk of HFD feeding (37). The discrepancy between these reports and our present observations may be explained, at least in part, by differences in the duration of exposure to HFD. We propose that hypothalamic S6K plays a predominant role in the onset of hypothalamic insulin resistance during HFD feeding, while prolonged nutrient excess results in the activation of inflammatory pathways, including JNK phosphorylation (35) and/or PTP-1B (37), which may support the maintenance of long-term hypothalamic insulin resistance.

Results from genetic deletion studies suggest that hypothalamic IRS-2 is more critical than IRS-1 in mediating the hypothalamic

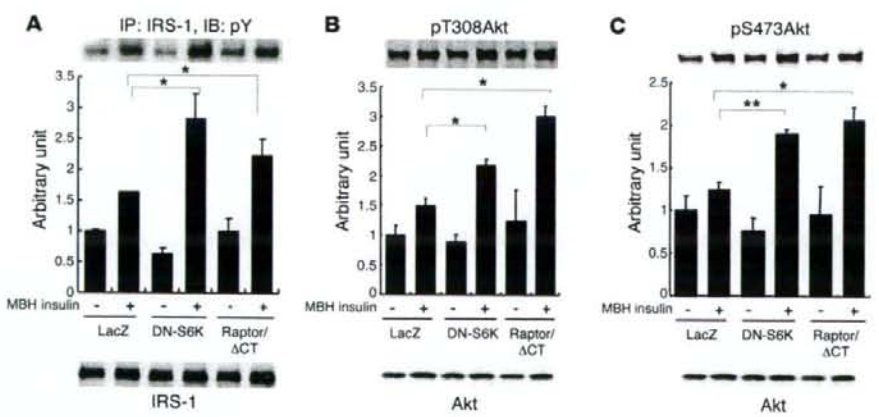

Figure 10

Insulin signaling in the MBH is improved by adenoviral inhibition of the mTOR/S6K pathway. Rats were fed NC or HFD for 1 d, and insulin signaling was analyzed 15 min after infusion of insulin (4 μU total) into the MBH. The tyrosine phosphorylation of IRS-1 (**A**) and phosphorylation of Akt at Thr308 (**B**) and at Ser473 (**C**) by insulin were enhanced in response to the overexpression of DN-S6K or Raptor/ΔCT. All graphs show the ratio of phosphoproteins to total proteins. $^{*}P < 0.05$; $^{**}P < 0.01$.

regulation of metabolism (38–40). In contrast, IRS-1 appears to be more clearly involved in negative feedback arising from the mTOR/S6K pathway (10, 12, 13, 25, 41, 42). Based on our present findings, we speculate that an mTOR/S6K/IRS-1 negative feedback pathway plays a dominant role in the early phase of HFD-induced hypothalamic insulin resistance.

Our observations support the idea that the mTOR/S6K pathway is critical for nutrient sensing in the arcuate nucleus. Activation of this pathway may have distinct and dissociable effects on 2 aspects of nutrient availability: glucose homeostasis and energy balance. Although Cota et al. have previously suggested that central administration of leucine reduces subsequent food intake by activating TORC1 pathway in the hypothalamus (43), we detected no significant differences in body weight after MBH injections, catheterization surgery, or clamping (Supplemental Table 1). This could be explained by divergence of TORC1 targets: while MBH IRS-1 is implicated in the ability of S6K to affect HGP, the downstream effectors of TORC1 on food intake remain unknown. Alternatively, there could be heterogeneity of responses within the MBH cell populations. While adenoviral injection allows rapid changes to be produced, and thereby circumvents developmental effects, it fails to distinguish among different cell populations (neurons versus glial cells, and neuronal subpopulations). Thus, further studies with conditional knockouts will be required.

In summary, our present findings indicate that diet-induced insulin resistance develops very rapidly in the hypothalamus in concert with decreased stimulation of IRS-1 and Akt by insulin and increased S6K activity. Our findings suggest that inhibition of S6K within the MBH may prevent the earliest stage of diet-induced insulin resistance. The phenotype of systemic S6K knockout mice (13) might result from enhanced hypothalamic insulin sensitivity, at least in part. Taken together with recent reports on the role of hypothalamic mTOR in the regulation of feeding behavior (43), these findings may lead to new therapeutic avenues for targeting metabolic syndrome and diabetes.

Methods

Animal preparation. All study protocols were reviewed and approved by the Institutional Animal Care and Use Committee of the Albert Einstein College of Medicine. We used 208 male Sprague-Dawley rats weighing 280–310 g (Charles River Breeding Laboratories). The rats were housed in individual cages and subjected to a standard light/dark cycle and NC diet (3.00 kcal/g, catalog no. 5001; Purina Mills Inc.). At 12 d before the clamp or insulin bolus studies, bilateral cannulae targeting the MBH were stereotactically implanted (3.0 mm caudal to the bregma, 9.4 mm below the skull surface, ±0.4 mm lateral to the midline). The adenoviral vector (2×10^8 pfu in 2 μl/side over a 20-min period) was infused bilaterally using paired 30-gauge stainless steel injectors extending 1.0 mm from the distal tips of the guide cannulae, and injectors were removed 20 min after completion of the 20-min injection. After 7 d, rats for clamp studies were implanted with additional catheters in the right internal jugular vein and left carotid artery as previously described (44). In the HFD-fed group, the NC diet was discontinued the day before the clamp study and substituted with a HFD (NC plus 10% lard, 5.14 kcal/g; ref. 44).

Clamp studies. Rats received 20 g NC or HFD the evening before the clamp studies in order to achieve comparable postabsorptive status in all animals. Body weight at the first surgery, second surgery, and the day of clamping as well as plasma insulin and blood glucose levels before the start of MBH insulin, during the basal period (60–120 min), and during the clamp period (210–240 min) are shown in Supplemental Table 1. The protocol of basal pancreatic clamp studies (Figure 2A) was as follows. At 0 min, a bilateral MBH infusion of insulin (5.6 nU/min/side in saline with 0.1% BSA) or vehicle was started. Following an equilibration period (0–120 min), a primed continuous infusion of [3-^{3}H]-glucose (40 μCi bolus, 0.4 μCi/min; New England Nuclear) was begun. Samples for determination of [3-^{3}H]-glucose-specific activity were obtained at 10-min intervals. Finally, a pancreatic insulin clamp with infusion of 1 mU/kg/min (~20 μU/ml) insulin and 3 μg/kg/min somatostatin was initiated at 240 min and continued for 2 h. During the clamp period, 25% glucose solution was infused at a variable rate to maintain the plasma glucose concentration at approximately 8 mM. We injected 14C-lactate during the last 10 min of the clamp period for the gluconeogenesis analysis, but a technical problem prevented us from analyzing these samples for this study. The hyperinsulinemic clamp study consisted of a 2-h basal and a 2-h insulin clamp period with continuous infusion of insulin at 3 mU/kg/min. At the completion of these clamp studies, rats were anesthetized, and tissue samples were freeze-clamped in situ with aluminum tongs precooled in liquid nitrogen. The MBH was dissected and processed for immunoprecipitation, immunoblot, or S6K assay.

Subcloning and adenovirus preparation. Rat p70 S6K 1 (shorter form of Rps6kb1) cDNA was subcloned using RT-PCR from the rat liver, and human Raptor cDNA was subcloned from a human cDNA library. N-terminal Flag and myc tag, mutations in S6K at F5A, K100Q, T389E, and RSPRR to ASPAA (aa 410–414); and truncation of Raptor at aa 905 were introduced using PCR-based mutagenesis, with confirmation of whole sequences. Adenoviruses for S6K mutants were generated using the Adeno-X expression system version 1 (BD Biosciences – Clontech), with a substitution of the promoter in the shuttle vector from CMV to CAG (45). Raptor/ΔCT and LacZ adenoviruses were prepared as previously described (32, 45). Adenoviruses were amplified in 293 cells and purified with an Adenopure kit (Puresyn Inc.). Adenoviral titers were measured by end point dilution assay with 1:3 serial dilutions on a 96-well plate of HEK293 cells.

MBH insulin bolus studies. Food was removed the morning of the studies. After a 5-h fast, anesthetized rats received 2 μU/side insulin infusion for 5 min and were sacrificed 15 min after the start of the infusion. This total dose is the same as that used for the insulin clamp study. In the S6K assay of NC compared with 1-d HFD feeding with or without insulin infusion (Figure 3B), the MBH was harvested 40 min after the start of insulin or vehicle infusion. The brains were isolated, and the MBH was sampled by dissecting a wedge of tissue including the entire mediolateral and dorsoventral extent of the arcuate nuclei while minimizing ventromedial nucleus tissue. The MBH was sonicated in 400 μl ice-chilled lysis buffer (50 mM HEPES, pH 7.7; 100 mM sodium chloride; 50 mM sodium fluoride; 40 mM β-glycerophosphate; 10 mM sodium pyrophosphate; 1 mM EDTA; 1 mM EGTA; 10 mM sodium orthovanadate; 2 mM PMSF; 1% NP-40; and complete inhibitor cocktail from Roche Diagnostics) for 10 s. The supernatant obtained by a centrifugation at 12,000 *g* for 15 min was taken as the tissue lysate and assayed as for protein concentration with a BCA kit (Pierce). The total MBH protein amount from 1 animal was approximately 500–800 μg. Tissue lysates were adjusted to the same protein concentration and used for immunoprecipitation or immunoblotting.

Portal insulin bolus study. Food was removed the morning of the studies. After a 5-h fast, rats were anesthetized, the abdomen was opened, and a catheter was inserted into the portal vein. Insulin (1 U/kg) was infused within 30 s, and the liver was harvested 3 min after the start of this infusion, then homogenized in a 10× volume of the same lysis buffer as that used in the MBH insulin study. Processing of the homogenate was same as that of the MBH signaling study.

TORC1 signaling studies in GT1-7 hypothalamic cells. The GT1-7 cell line was kindly provided by P. Mellon (UCSD, San Diego, California, USA). Cells at

approximately 80% confluence were infected with adenovirus, each at MOI 300. After 48 h, cells that had been serum starved for 16 h were stimulated with 0, 1, 10, or 100 nM insulin for 30 min, harvested in 1× Laemmli buffer, boiled, and processed for Western blotting. All site-specific phosphoserine antibodies, anti-Raptor, and anti-S6 antibodies were from Cell Signaling. Anti-β-actin antibody was from Novus Biologicals.

Immunoprecipitation and Western blotting. MBH lysates (60 μg for phosphotyrosine; 150 μg for IRS-1 or IRS-2; or 100 μg for Flag) were incubated with 5 μg anti-phosphotyrosine (4G10; Upstate), anti-IRS-1 or anti-IRS-2 antibodies (Upstate), or anti-M2 Flag (Sigma-Aldrich) for 3 h (phosphotyrosine or IRS) or overnight (Flag) at 4°C. Protein G or protein A Sepharose beads were added, followed by agitation for 1 h. Immunoprecipitants were washed with the lysis buffer and boiled in Laemmli buffer. Total tissue lysates were also boiled in Laemmli buffer, and samples were electrophoresed in 4%–15% Tris-HCl precast gradient gel (BioRad) and transferred to a nitrocellulose membrane. To detect tyrosine phosphorylation of IR or IRS, the membrane was blocked with Tris-buffered saline with Tween 20 plus 3% BSA and incubated with anti-IRβ (1:1,000; Santa Cruz Biotechnology Inc.) or anti-phosphotyrosine (1:10,000, 4G10; Upstate) at 4°C overnight, followed by incubation with HRP-conjugated secondary antibody for 1 h. The signal was then detected with ECL (GE Healthcare). For other samples, the membrane was blocked with Odyssey blocking buffer (Licor Biosciences), followed by incubation with primary antibodies (anti-S6K, 1:1,000; Upstate; anti-total Akt, anti-phospho-Akt, anti-phospho-JNK, or anti-myc, 1:1,000; Cell Signaling; anti-PTP-1B, 1:200; Santa Cruz Biotechnology Inc.; anti-M5-Flag or anti-β-gal, 1:1,000; Sigma-Aldrich) overnight at 4°C, then by incubation with IRDye-conjugated secondary antibodies, and the signal was finally detected using the Licor Odyssey system.

S6K activity assay. The S6K assay kit (Upstate) was used with minor modifications. Briefly, 200 μg tissue lysate was incubated with 3 μg anti-S6K antibody and 30 μl protein A Sepharose beads in modified buffer A (50 mM Tris, pH 7.5; 1 mM EDTA; 1 mM EGTA; 2 mM sodium orthovanadate; 0.1% 2-mercaptoethanol; 1% Triton X-100; 50 mM sodium fluoride; 10 mM sodium pyrophosphate; 10 mM β-glycerophosphate; 0.2 mM PMSF; and complete inhibitor cocktail from Roche Diagnostics) and agitated for 2 h at 4°C, then washed 3 times with the same buffer and twice with Assay Dilution Buffer I (Upstate), then incubated with synthetic substrate peptide (KKRNRTLTK) and [γ-^{32}P]ATP at 30°C for 10 min with continuous agitation. After a brief spin down, supernatants were spotted onto W81 filter paper, washed with diluted phosphoric acid, and counted with a scintillation counter.

Brain micropunch. Brain micropunches of individual hypothalamic nuclei were performed as described previously (46).

Statistics. All values are mean ± SEM. Western blots were quantified – or scanned from film, then quantified – using a Licor Odyssey system. Comparisons among groups were made using ANOVA or unpaired Student's *t* test as appropriate. A *P* value less than 0.05 was considered significant.

Acknowledgments

We wish to thank Bing Liu, Hong Zhang, Zhiping Wu, Clive Baveghems, and Stanislaw Gaweda for expert technical assistance. H. Ono is a recipient of a 2005 research fellowship from the Sankyo Foundation of Life Science and a 2007 research fellowship from Uehara Memorial Foundation. This work was supported by NIH grant DK045024 and by the American Diabetes Association to L. Rossetti; by NIH grant DK066618 and by the Skirball Institute for Nutrient Sensing to G.J. Schwartz; and by NIH grant DK020541 to the Albert Einstein College of Medicine Diabetes Research and Training Center.

Received for publication October 19, 2007, and accepted in revised form May 28, 2008.

Address correspondence to: Hiraku Ono, Albert Einstein College of Medicine, 1300 Morris Park Avenue, New York, New York 10461, USA. Phone: (718) 430-2348; Fax: (718) 430-8557; E-mail: hono@aecom.yu.edu.

Alessandro Pocai's and Luciano Rossetti's present address is: Merck Research Laboratories, Rahway, New Jersey, USA.

1. Hay, N., and Sonenberg, N. 2004. Upstream and downstream of mTOR. *Genes Dev.* **18**:1926–1945.
2. Fingar, D.C., and Blenis, J. 2004. Target of rapamycin (TOR): an integrator of nutrient and growth factor signals and coordinator of cell growth and cell cycle progression. *Oncogene.* **23**:3151–3171.
3. Corradetti, M.N., and Guan, K.L. 2006. Upstream of the mammalian target of rapamycin: do all roads pass through mTOR? *Oncogene.* **25**:6347–6360.
4. Avruch, J., et al. 2006. Insulin and amino-acid regulation of mTOR signaling and kinase activity through the Rheb GTPase. *Oncogene.* **25**:6361–6372.
5. Inoki, K., Zhu, T., and Guan, K.L. 2003. TSC2 mediates cellular energy response to control cell growth and survival. *Cell.* **115**:577–590.
6. Byfield, M.P., Murray, J.T., and Backer, J.M. 2005. hVps34 is a nutrient-regulated lipid kinase required for activation of p70 S6 kinase. *J. Biol. Chem.* **280**:33076–33082.
7. Nobukuni, T., et al. 2005. Amino acids mediate mTOR/raptor signaling through activation of class 3 phosphatidylinositol 3OH-kinase. *Proc. Natl. Acad. Sci. U. S. A.* **102**:14238–14243.
8. Findlay, G.M., Yan, L., Procter, J., Mieulet, V., and Lamb, R.F. 2007. A MAP4 kinase related to Ste20 is a nutrient-sensitive regulator of mTOR signalling. *Biochem. J.* **403**:13–20.
9. Harrington, L.S., Findlay, G.M., and Lamb, R.F. 2005. Restraining PI3K: mTOR signalling goes back to the membrane. *Trends Biochem. Sci.* **30**:35–42.
10. Manning, B.D. 2004. Balancing Akt with S6K: implications for both metabolic diseases and tumorigenesis. *J. Cell Biol.* **167**:399–403.
11. Fisher, T.L., and White, M.F. 2004. Signaling pathways: the benefits of good communication. *Curr. Biol.* **14**:R1005–R1007.
12. Um, S.H., D'Alessio, D., and Thomas, G. 2006. Nutrient overload, insulin resistance, and ribosomal protein S6 kinase 1, S6K1. *Cell Metab.* **3**:393–402.
13. Um, S.H., et al. 2004. Absence of S6K1 protects against age- and diet-induced obesity while enhancing insulin sensitivity. *Nature.* **431**:200–205.
14. Gelling, R.W., et al. 2006. Insulin action in the brain contributes to glucose lowering during insulin treatment of diabetes. *Cell Metab.* **3**:67–73.
15. Inoue, H., et al. 2006. Role of hepatic STAT3 in brain-insulin action on hepatic glucose production. *Cell Metab.* **3**:267–275.
16. Konner, A.C., et al. 2007. Insulin action in AgRP-expressing neurons is required for suppression of hepatic glucose production. *Cell Metab.* **5**:438–449.
17. Obici, S., Zhang, B.B., Karkanias, G., and Rossetti, L. 2002. Hypothalamic insulin signaling is required for inhibition of glucose production. *Nat. Med.* **8**:1376–1382.
18. Pocai, A., et al. 2005. Hypothalamic K(ATP) channels control hepatic glucose production. *Nature.* **434**:1026–1031.
19. Kraegen, E.W., et al. 1991. Development of muscle insulin resistance after liver insulin resistance in high-fat-fed rats. *Diabetes.* **40**:1397–1403.
20. Wang, J., et al. 2001. Overfeeding rapidly induces leptin and insulin resistance. *Diabetes.* **50**:2786–2791.
21. Lam, T.K., Gutierrez-Juarez, R., Pocai, A., and Rossetti, L. 2005. Regulation of blood glucose by hypothalamic pyruvate metabolism. *Science.* **309**:943–947.
22. Obici, S., et al. 2002. Central administration of oleic acid inhibits glucose production and food intake. *Diabetes.* **51**:271–275.
23. Holz, M.K., and Blenis, J. 2005. Identification of S6 kinase 1 as a novel mammalian target of rapamycin (mTOR)-phosphorylating kinase. *J. Biol. Chem.* **280**:26089–26093.
24. Schalm, S.S., Tee, A.R., and Blenis, J. 2005. Characterization of a conserved C-terminal motif (RSPRR) in ribosomal protein S6 kinase 1 required for its mammalian target of rapamycin-dependent regulation. *J. Biol. Chem.* **280**:11101–11106.
25. Shah, O.J., and Hunter, T. 2006. Turnover of the active fraction of IRS1 involves raptor-mTOR- and S6K1-dependent serine phosphorylation in cell culture models of tuberous sclerosis. *Mol. Cell. Biol.* **26**:6425–6434.
26. Tzatsos, A., and Kandror, K.V. 2006. Nutrients suppress phosphatidylinositol 3-kinase/Akt signaling via raptor-dependent mTOR-mediated insulin receptor substrate 1 phosphorylation. *Mol. Cell. Biol.* **26**:63–76.
27. Shah, O.J., Wang, Z., and Hunter, T. 2004. Inappropriate activation of the TSC/Rheb/mTOR/S6K cassette induces IRS1/2 depletion, insulin resistance, and cell survival deficiencies. *Curr. Biol.* **14**:1650–1656.
28. Tang, H., et al. 2001. Amino acid-induced transla-

tion of TOP mRNAs is fully dependent on phosphatidylinositol 3-kinase-mediated signaling, is partially inhibited by rapamycin, and is independent of S6K1 and rpS6 phosphorylation. *Mol. Cell. Biol.* **21**:8671–8683.
29. Wu, Q., Zhang, Y., Xu, J., and Shen, P. 2005. Regulation of hunger-driven behaviors by neural ribosomal S6 kinase in Drosophila. *Proc. Natl. Acad. Sci. U. S. A.* **102**:13289–13294.
30. Hara, K., et al. 2002. Raptor, a binding partner of target of rapamycin (TOR), mediates TOR action. *Cell.* **110**:177–189.
31. Nojima, H., et al. 2003. The mammalian target of rapamycin (mTOR) partner, raptor, binds the mTOR substrates p70 S6 kinase and 4E-BP1 through their TOR signaling (TOS) motif. *J. Biol. Chem.* **278**:15461–15464.
32. Koketsu, Y., et al. 2008. Hepatic overexpression of a dominant negative form of raptor enhances Akt phosphorylation and restores insulin sensitivity in K/KAy mice. *Am. J. Physiol. Endocrinol. Metab.* **294**:E719–E725.
33. Samuel, V.T., et al. 2004. Mechanism of hepatic insulin resistance in non-alcoholic fatty liver disease. *J. Biol. Chem.* **279**:32345–32353.
34. Anai, M., et al. 1999. Enhanced insulin-stimulated activation of phosphatidylinositol 3-kinase in the liver of high-fat-fed rats. *Diabetes.* **48**:158–169.
35. Prada, P.O., et al. 2005. Western diet modulates insulin signaling, c-Jun N-terminal kinase activity, and insulin receptor substrate-1ser307 phosphorylation in a tissue-specific fashion. *Endocrinology.* **146**:1576–1587.
36. Ueno, M., et al. 2005. Regulation of insulin signalling by hyperinsulinaemia: role of IRS-1/2 serine phosphorylation and the mTOR/p70 S6K pathway. *Diabetologia.* **48**:506–518.
37. Zabolotny, J.M., et al. 2008. Protein tyrosine phosphatase 1B (PTP1B) expression is induced by inflammation in vivo. *J. Biol. Chem.* **283**:14230–14241.
38. Choudhury, A.I., et al. 2005. The role of insulin receptor substrate 2 in hypothalamic and beta cell function. *J. Clin. Invest.* **115**:940–950.
39. Kubota, N., et al. 2004. Insulin receptor substrate 2 plays a crucial role in beta cells and the hypothalamus. *J. Clin. Invest.* **114**:917–927.
40. Lin, X., et al. 2004. Dysregulation of insulin receptor substrate 2 in beta cells and brain causes obesity and diabetes. *J. Clin. Invest.* **114**:908–916.
41. Gual, P., Le Marchand-Brustel, Y., and Tanti, J.F. 2005. Positive and negative regulation of insulin signaling through IRS-1 phosphorylation. *Biochimie.* **87**:99–109.
42. Tremblay, F., et al. 2005. Overactivation of S6 kinase 1 as a cause of human insulin resistance during increased amino acid availability. *Diabetes.* **54**:2674–2684.
43. Cota, D., et al. 2006. Hypothalamic mTOR signaling regulates food intake. *Science.* **312**:927–930.
44. Pocai, A., et al. 2006. Restoration of hypothalamic lipid sensing normalizes energy and glucose homeostasis in overfed rats. *J. Clin. Invest.* **116**:1081–1091.
45. Miyake, S., et al. 1996. Efficient generation of recombinant adenoviruses using adenovirus DNA-terminal protein complex and a cosmid bearing the full-length virus genome. *Proc. Natl. Acad. Sci. U. S. A.* **93**:1320–1324.
46. Obici, S., Feng, Z., Arduini, A., Conti, R., and Rossetti, L. 2003. Inhibition of hypothalamic carnitine palmitoyltransferase-1 decreases food intake and glucose production. *Nat. Med.* **9**:756–761.

Am J Physiol Endocrinol Metab 294: E719–E725, 2008.
First published February 12, 2008; doi:10.1152/ajpendo.00253.2007.

Hepatic overexpression of a dominant negative form of raptor enhances Akt phosphorylation and restores insulin sensitivity in K/KAy mice

Yuko Koketsu,[1] Hideyuki Sakoda,[1] Midori Fujishiro,[1] Akifumi Kushiyama,[1] Yasushi Fukushima,[1] Hiraku Ono,[1] Motonobu Anai,[2] Takako Kikuchi,[1] Takeshi Fukuda,[1] Hideaki Kamata,[4] Nanao Horike,[3] Yasunobu Uchijima,[3] Hiroki Kurihara,[3] and Tomoichiro Asano[4]

[1]*Department of Internal Medicine, Graduate School of Medicine, University of Tokyo;* [2]*Institute for Adult Disease, Asahi Life Foundation;* [3]*Department of Physiological Chemistry and Metabolism, Graduate School of Medicine, University of Tokyo, Tokyo; and* [4]*Department of Medical Science, Graduate School of Medicine, University of Hiroshima, Hiroshima, Japan*

Submitted 28 August 2007; accepted in final form 11 February 2008

Koketsu Y, Sakoda H, Fujishiro M, Kushiyama A, Fukushima Y, Ono H, Anai M, Kikuchi T, Fukuda T, Kamata H, Horike N, Uchijima Y, Kurihara H, Asano T. Hepatic overexpression of a dominant negative form of raptor enhances Akt phosphorylation and restores insulin sensitivity in K/KAy mice. *Am J Physiol Endocrinol Metab* 294: E719–E725, 2008. First published February 12, 2008; doi:10.1152/ajpendo.00253.2007.—Several serine/threonine kinases reportedly phosphorylate serine residues of IRS-1 and thereby induce insulin resistance. In this study, to investigate the effect of mTOR/raptor on insulin signaling and metabolism in K/KAy mice with genetic obesity-associated insulin resistance, a dominant negative raptor, COOH-terminally deleted raptor (raptor-ΔC_T), was overexpressed in the liver via injection of its adenovirus into the circulation. Hepatic raptor-ΔC_T expression levels were 1.5- to 4-fold that of endogenously expressed raptor. Glucose tolerance in raptor-ΔC_T-overexpressing mice improved significantly compared with that of LacZ-overexpressing mice. Insulin-induced activation of p70S6 kinase ($p70^{S6k}$) was significantly suppressed in the livers of raptor-ΔC_T overexpressing mice. In addition, insulin-induced IRS-1, Ser^{307}, and $Ser^{636/639}$ phosphorylations were significantly suppressed in the raptor-ΔC_T-overexpressing liver, whereas tyrosine phosphorylation of IRS-1 was increased. PI 3-kinase activation in response to insulin stimulation was increased approximately twofold, and Akt phosphorylation was clearly enhanced under both basal and insulin-stimulated conditions in the livers of raptor-ΔC_T mice. Thus, our data indicate that suppression of the mTOR/$p70^{S6k}$ pathway leads to improved glucose tolerance in K/KAy mice. These observations may contribute to the development of novel antidiabetic agents.

insulin receptor substrate-1; insulin resistance

THE MAMMALIAN TARGET OF RAPAMYCIN (mTOR) is a Ser/Thr kinase that belongs to the phosphatidylinositol (PI) kinase-related protein kinase family, which regulates cell growth and metabolism (7, 21). The mTOR signaling network consists of two major branches, each of which are mediated by a specific mTOR complex (mTORC) (27). The rapamycin-sensitive mTORC1 consists of mTOR, raptor, and mLST8 (also known as GβL) and regulates cell growth through effectors such as ribbosomal protein S6 kinase (S6K)1 and eukaryotic initiation factor 4E-binding protein-1 (4E-BP1) (4, 10). The rapamycin-insensitive mTORC2 contains mTOR, rictor, and mLST8 and regulates cellular proliferation through Akt (22), cytoskeleton organization through protein kinase Cα (20), and the small GTPases Rho and Rac (9).

Raptor is a large protein (150 kDa) containing a highly conserved, amino-terminal domain followed by several HEAT repeats and seven carboxy-terminal WD40 repeats (4). A number of groups (2, 12, 23) have proposed that raptor acts as an adaptor to recruit substrates p70 S6 kinase ($p70^{S6k}$) and 4E-BP1 to mTOR. Recent studies (6, 24, 26) have shown the existence of a negative feedback loop from the nutrient-sensitive TSC-mTOR-S6K1 pathway to the upstream, insulin-responsive insulin receptor substrate (IRS)-PI 3-kinase-PDK1-Akt pathway. S6K1 knockout mice were shown to be hypoinsulinemic with a decrease in β-cell mass (17). Moreover, S6K1-deficient mice are hypersensitive to insulin due to loss of the negative feedback loop from S6K1 to IRS-1 and are protected from age- and diet-induced obesity (26). Meanwhile, in genetic models of obesity, such as K/KAy and *ob/ob* mice, insulin signaling is suppressed with increased phosphorylation of Ser^{307} and $Ser^{636/639}$ in IRS-1 (26). In such mice, the activities of JNK and mTOR/S6K1, which can phosphorylate serine residue(s) of IRS-1, are reportedly elevated (8, 26).

In the present study, to elucidate the contribution of mTORC1, we overexpressed a dominant negative raptor, COOH-terminally deleted raptor (raptor-ΔC_T), using adenovirus gene transfer into the livers of K/KAy mice. Since raptor-ΔC_T binds S6K but not mTOR, raptor-ΔC_T overexpression inhibits mTOR/S6K signaling (12, 25). Under these conditions, we were able to evaluate the contribution of the mTORC1 pathway to glucose tolerance as well as signal transduction. Herein, we present data suggesting inhibition of mTORC1 to significantly enhance insulin signaling, particularly Akt activation, and thereby to ultimately improve glucose tolerance in K/KAy mice.

MATERIALS AND METHODS

Materials. Affinity-purified antibodies against IRS-1, IRS-2, phosphorylated tyrosine (4G10), S6K, and Akt/protein kinase B were prepared as previously described (11). Anti-Flag tag antibody was purchased from Sigma-Aldrich (St. Louis, MO). The antibodies against raptor, phospho-Thr^{389} of S6K, phospho-Ser^{307} and phospho-$Ser^{636/639}$ of IRS-1, phospho-$Thr^{37/46}$ and phospho-Thr^{70} of 4E-BP1, and phospho-Ser^{473} and phospho-Thr^{308} of Akt, were purchased from Cell Signaling Technology.

Address for reprint requests and other correspondence: T. Asano, Dept. of Medical Science, Graduate School of Medicine, Univ. of Hiroshima, 1-2-3 Kasumi, Minami-ku, Hiroshima City, Hiroshima, Japan 734-8553 (e-mail: asano-tky@umin.ac.jp).

The costs of publication of this article were defrayed in part by the payment of page charges. The article must therefore be hereby marked "*advertisement*" in accordance with 18 U.S.C. Section 1734 solely to indicate this fact.

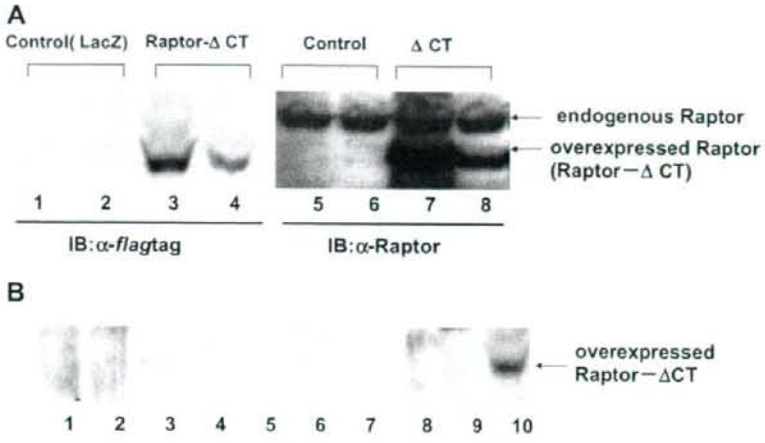

Fig. 1. The adenovirus of dominant negative raptor, COOH-terminally deleted raptor (raptor-ΔC_T). *A*: the expression levels of endogenous raptor and overexpressed raptor-ΔC_T in the livers of K/KAy mice and controls. *B*: immunoblotting (IB) of overexpressed raptor-ΔC_T in various tissues with anti-Flag tag antibody. Each tissue (30 μg), from raptor-ΔC_T-overexpressing mice, was electrophoresed and immunoblotted with anti-Flag tag antibody. *Blot 1*: brain; *blot 2*: lung; *blot 3*: heart; *blot 4*: spleen; *blot 5*: pancreas; *blot 6*: kidney; *blot 7*: fat; *blot 8*: muscle; *blot 9*: testis; *blot 10*: liver.

Adenoviruses and animals. Raptor-ΔC_T (amino acids 1–905), a dominant negative raptor, was constructed by deleting the COOH terminus of raptor. PCR was performed to amplify human raptor cDNA using a cDNA library obtained from HEK293 as a template and oligonucleotides on the basis of its reported sequence (4) as primers, yielding raptor cDNA encompassing the entire coding region. Raptor-ΔC_T (Δ, 906–1335) was generated by standard PCR-based strategies. The construct was designed to contain an Myc tag and a Flag tag at the NH_2 terminus. Recombinant adenovirus expressing β-galactosidase [i.e., the *E. coli* β -galactosidase gene (LacZ)] and COOH-terminally deleted raptor (raptor-ΔC_T) were generated, purified, and concentrated using cesium chloride ultracentrifugation, as reported previously (19). Adenovirus encoding LacZ served as a control. Male K/KAy mice, 9 wk of age, were obtained from Nippon Bio-Supp. Center (Tokyo, Japan). They were injected via the tail vein with adenovirus at a dose of 2.5×10^7 plaque-forming units/g body wt. Four days after adenovirus injection, the following experiments were performed.

Serum glucose and lipid profiles. Blood glucose was measured with a portable blood glucose monitor, Glutest-Ace R (Sanwa Kagaku Kenkyusho, Nagoya, Japan). The plasma insulin level was determined with an enzymatic immunoassay kit (Shibayagi). Serum triglyceride, cholesterol, and free fatty acids were assayed with the Triglyceride E-test, Cholesterol E-test, and NEFA C test (all from Wako Chemicals), respectively.

Intraperitoneal glucose tolerance tests. Mice were fasted for 14 h, followed by blood sampling and intraperitoneal injection of glucose (2 g/kg body wt). Whole venous blood was obtained from the tail vein at the indicated time points after the glucose load. Blood glucose was measured with a portable blood glucose monitor, as described above. We calculated the areas under the curve for glucose for each group and then compared the values obtained using Student's *t*-test.

In vivo insulin stimulation. In vivo insulin stimulation was performed as described previously (15). Mice were anesthetized with pentobarbital sodium, 0.2 ml of blood was collected from the heart, and the same amount of normal saline (0.9% NaCl), with or without insulin (1 unit/kg body wt), was then injected into the heart. The livers were removed 5 or 20 min later and immediately homogenized with a Polytron homogenizer in 10 volumes of solubilization buffer [*buffer A*: 1% Triton X-100, 20 mM Tris (pH 7.5), 150 mM NaCl, 10% glycerol, 1 mM EDTA, 100 mM sodium pyrophosphate, 100 mM sodium fluoride, 20 mM β-glycerophosphate, 2 mM sodium vanadate, 1 mM phenylmethylsulfonyl fluoride (PMSF), and 0.02 mg/ml aprotinin; *buffer B*: 137 mM NaCl, 20 mM Tris (pH 7.5), 1 mM $MgCl_2$ 1 mM $CaCl_2$, 10% glycerol, 1% NP-40, 0.05 mM sodium vanadate, 1 mM PMSF; *buffer C*: 20 mM Tris (pH 7.5), 20 mM NaCl, 1 mM EDTA, 5 mM EGTA, 1% CHAPS, 20 mM β-glycerophosphate, 1 mM sodium vanadate, 1 mM PMSF, 1 mM DTT]. The extract was centrifuged at 20,000 *g* for 15 min at 4°C, and the supernatants were used as samples for immunoprecipitation, immunoblotting (*buffer A*), or kinase assay of PI 3-kinase (*buffer B*) and S6K (*buffer C*).

Immunoprecipitation and immunoblotting. Supernatants containing equal amounts of protein (10 mg) were incubated with anti-IRS-1 and anti-S6K antibodies (3 μg/ml each) and then incubated with 45 μl of protein A- and G-Sepharose. The samples were washed and then boiled in Laemmli sample buffer containing 100 mM DTT. SDS-PAGE and immunoblotting were carried out using enhanced chemiluminescenece (ECL detection kit; Amersham), and representative blots were obtained by exposing the films. The bands were quantitatively analyzed using Molecular Imager FX (Bio-Rad) without exposure of the films.

Measurement of PI 3-kinase. For PI 3-kinase assay, the supernatants containing equal amounts of protein were immunoprecipitated for 2 h at 4°C with anti-IRS-1 or 4G10 antibody and protein A- or G-Sepharose. PI 3-kinase activities in the immunoprecipitates were assayed as described previously (14).

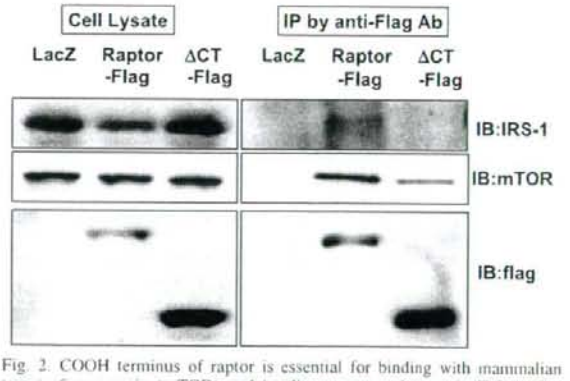

Fig. 2. COOH terminus of raptor is essential for binding with mammalian target of rapamycin (mTOR) and insulin receptor substrate-1 (IRS-1). For wild-type raptor, raptor-ΔC_T, and control (LacZ) gene transfer into HepG2 cells, the cells were incubated for 1 h in DMEM containing recombinant adenovirus. Two days later the cells were collected, and cell lysates were immunoprecipitated with Flag-tag antibody. Cell lysates and anti-Flag tag immunoprecipitates were immunoblotted with each (IRS-1, mTOR, and Flag) antibody as a probe. Representative results are shown. LacZ: $n = 3$; raptor: $n = 3$; raptor-ΔC_T: $n = 3$.

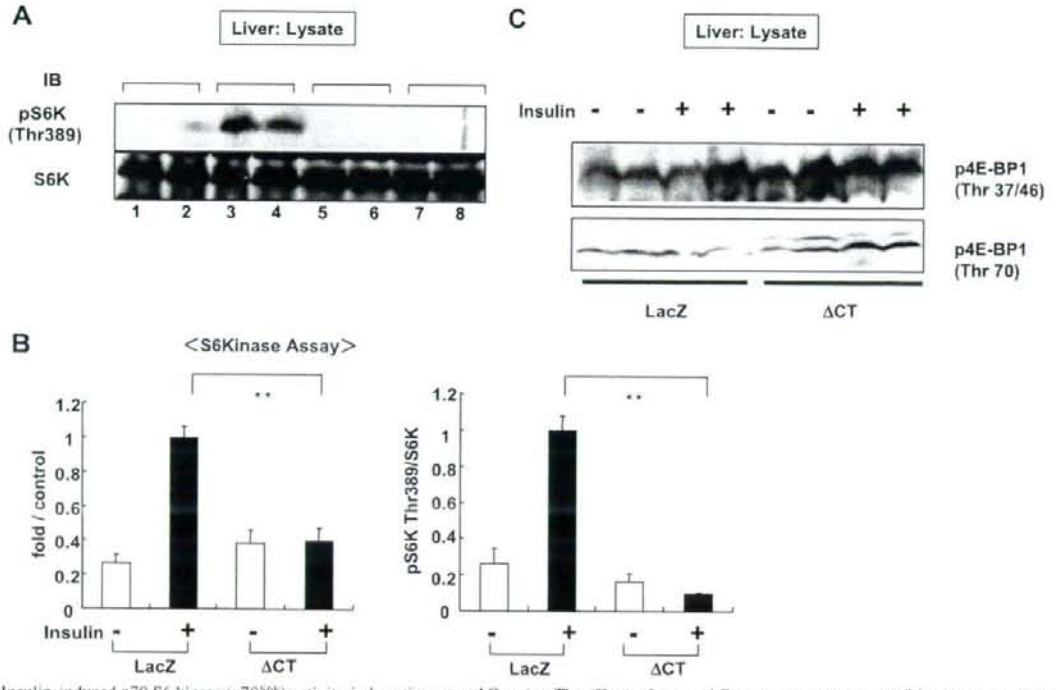

Fig. 3. Insulin-induced p70 S6 kinase ($p70^{S6k}$) activity in hepatic raptor-ΔC_T mice. The effects of raptor-ΔC_T overexpression on $p70^{S6k}$ and eukaryotic initiation factor 4E-binding protein-1 (4E-BP1) in the liver were investigated. *A*: IB of liver lysates with ribosomal S6 kinase (S6K) and phospho-S6K (Thr^{389}) antibodies revealed that insulin-induced activation of $p70^{S6k}$ was significantly depressed in the livers of raptor-ΔC_T mice. Three independent experiments were performed, and the panel shown is representative of the results. *B*: S6K assay showed insulin-induced activation of $p70^{S6k}$ to be markedly suppressed in the livers of raptor-ΔC_T overexpressing mice. LacZ: $n = 8$ (insulin$^+$: $n = 4$; insulin$^-$: $n = 4$); ΔC_T: $n = 8$ (insulin$^+$: $n = 4$; insulin$^-$: $n = 4$). $^{**}P < 0.01$. *C*: liver lysates were immunoblotted with phospho-4E-BP1 ($Thr^{37/46}$ and Thr^{70}) antibodies in 3 independent experiments, and representative results are shown. Both phosphorylations of 4E-BP1 are significantly enhanced by raptor-ΔC_T overexpression.

$p70^{S6k}$ assay. For $p70^{S6k}$ assay, the supernatants containing equal amounts of protein (10 mg) were immunoprecipitated for 2 h at 4°C with anti-S6K antibody and protein A-Sepharose. Kinase activity was analyzed using an S6K assay kit (Upstate Biotechnology, Lake Placid, NY), and the assay was carried out according to the manufacturer's instructions. In brief, the reaction mixture, containing 50 μM substrate peptide (KKRNRTLTK), inhibitor mixture [20 μM protein kinase C inhibitor peptide, 2 μM protein kinase A inhibitor peptide, and 20 μM compound R24571, an inhibitor of brain calmodulin-dependent phosphodiesterase in assay dilution buffer 1 (20 mM MOPS, pH 7.2, 25 mM β-glycerophosphate, 5 mM EGTA, 1 mM sodium orthovanadate, 1 mM dithiothreitol)], $p70^{S6k}$ (immunoprecipitates), and diluted [γ-^{32}P]ATP mixture were incubated for 10 min at 30°C. Then, 25 μl of the reaction mixture was spotted onto p81 phosphocellulose squares. Intensities of the resultant bands were determined using BAS2000 (Fuji Film).

Statistical analysis. Results are expressed as means ± SE. Comparisons were made using one-way ANOVA followed by the Tukey test and the unpaired Student *t*-test. Values of $P < 0.05$ were considered statistically significant.

RESULTS

Overexpression of raptor-ΔC_T markedly suppressed insulin-induced activation of $p70^{S6k}$ in the livers of K/KAy mice. To examine levels of endogenously expressed raptor and raptor-ΔC_T in the liver, we carried out immunoblotting with anti-Flag tag or anti-raptor antibody. Raptor-ΔC_T expressions were identified by immunoblotting with anti-Flag tag antibody in raptor-ΔC_T-overexpressing mice, but not in controls (Fig. 1). Immunoblotting with the anti-raptor antibody detected both endogenous raptor and overexpressed raptor-ΔC_T, and the levels of

Table 1. *Weights and metabolic profiles of LacZ and raptor-ΔC_T-overexpressing mice*

	LacZ	Raptor-ΔC_T
BW, g (*day 1*)	36.3±1.04	36.6±1.2
BW, g (*day 5*)	36.9±1.1	37±1.27
Liver/BW × 10^2 (*day 5*)	4.87±0.44	5.12±0.34
Fat/BW × 10^2 (*day 5*)	4±0.62	3.9±0.32
Heart/BW × 10^2 (*day 5*)	0.37±0.25	0.48±0.01
Kidney/BW × 10^2 (*day 5*)	0.94±0.62	1.28±0.02
FBS, mg/dl (*day 1*)	122±7.48	126±9.03
FBS, mg/dl (*day 5*)	160±6.31	140±8.37
T-cho, mg/dl (*day 5*)	123±10.8	125±7.96
TG, mg/dl (*day 5*)	197±83.2	200±48.2
NEFA, mEq/l (*day 5*)	0.79±0.13	0.88±0.22
Insulin, ng/ml (*day 5*)	2.36±1.78	0.91±0.34

Values are means ± SE. LacZ, control; raptor-ΔC_T, COOH-terminally deleted raptor; BW, body weight; FBS, fasting blood sugar; T-cho, total cholesterol; TG, triglyceride; NEFA, nonesterified fatty acid. The body weights, major organ weights, blood glucose levels, and lipid concentrations of LacZ and Raptor-ΔCT mice, before and 4 days after adenovirus injection, are shown. LacZ: $n = 8$; raptor-ΔC_T: $n = 8$.

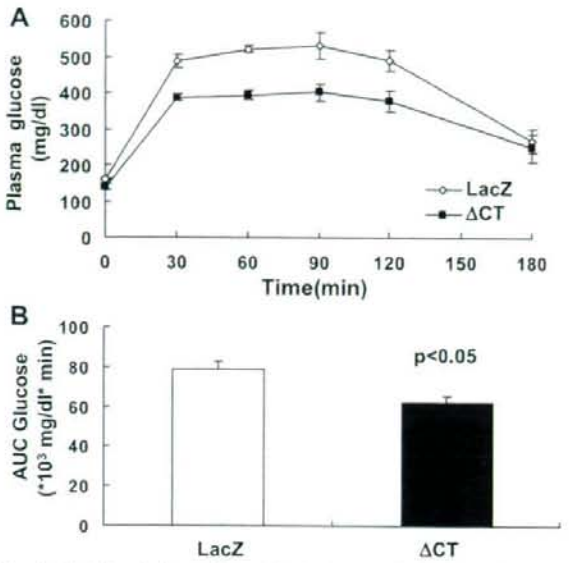

Fig. 4. Significantly lower glucose levels in raptor-ΔC_T mice after glucose tolerance test (GTT). Mice were fasted for 14 h, followed by blood sampling and intraperitoneal injection of glucose (2 g/kg body wt). *A*: whole venous blood was obtained from the tail vein at the indicated time points after the glucose load. *B*: areas under the curve (AUC) for glucose for each group were calculated and compared using the Student *t*-test. Intraperitoneal GTT revealed hepatic raptor-ΔC_T overexpression to improve glucose tolerance. LacZ: $n = 4$; raptor-ΔC_T: $n = 4$. $^*P < 0.05$.

raptor-ΔC_T were ~1.5- to fourfold that of endogenously expressed raptor (Fig. 1*A*). In addition, overexpression of raptor-ΔC_T was limited to the liver; i.e., none was detected by immunoblotting of other tissues (Fig. 1*B*). (Faint bands in the lung, heart, and kidney were nonspecific.) Next, we investigated the associations of wild-type raptor and raptor-ΔC_T with mTOR or IRS-1. As shown in Fig. 2, IRS-1 and mTOR were detected in the Flag-tagged raptor immunoprecipitates. In contrast, it was revealed that raptor-ΔC_T had lost the ability to associate with IRS-1, and the association of raptor-ΔC_T with mTOR was also much weaker than that of wild-type raptor. Thus, it was suggested that raptor-ΔC_T functions as a dominant negative construct.

Subsequently, the effect of raptor-ΔC_T overexpression on $p70^{S6k}$ activity was investigated in the liver. S6K assay and immunoblotting of liver lysates with S6K and phospho-S6K (Thr^{389}) antibodies revealed insulin-induced activation of $p70^{S6k}$ to be markedly suppressed in the livers of raptor-ΔC_T-overexpressing mice (Fig. 3, *A* and *B*). However, surprisingly, 4E-BP1 phosphorylations of both Thr^{37} and Thr^{46} were significantly increased by raptor-ΔC_T overexpression under both basal and insulin-stimulated conditions, and that of Thr^{70} was also increased in the insulin-stimulated state (Fig. 3*C*).

Weights and metabolic profiles of control (LacZ) and raptor-ΔC_T-overexpressing mice. The body weights, major organ weights, blood glucose levels, and lipid concentrations of raptor-ΔC_T mice did not differ from those of control mice either before or 4 days after adenovirus injection. Fasting serum insulin levels of raptor-ΔC_T mice were lower, but not significantly (Table 1).

Hepatic raptor-ΔC_T overexpressing mice showed a profound increase in glucose tolerance. To investigate the effect of hepatic raptor-ΔC_T overexpression on glucose tolerance, we performed intraperitoneal glucose tolerance tests (Fig. 4*A*). Blood glucose levels of raptor-ΔC_T mice were significantly lower than those of control mice (Fig. 4*B*).

Hepatic raptor-ΔC_T overexpression enhanced insulin signaling associated with decreased IRS-1 Ser^{307} and $Ser^{636/639}$ phosphorylation in K/KAy mice. As shown in Fig. 5*A*, there were no

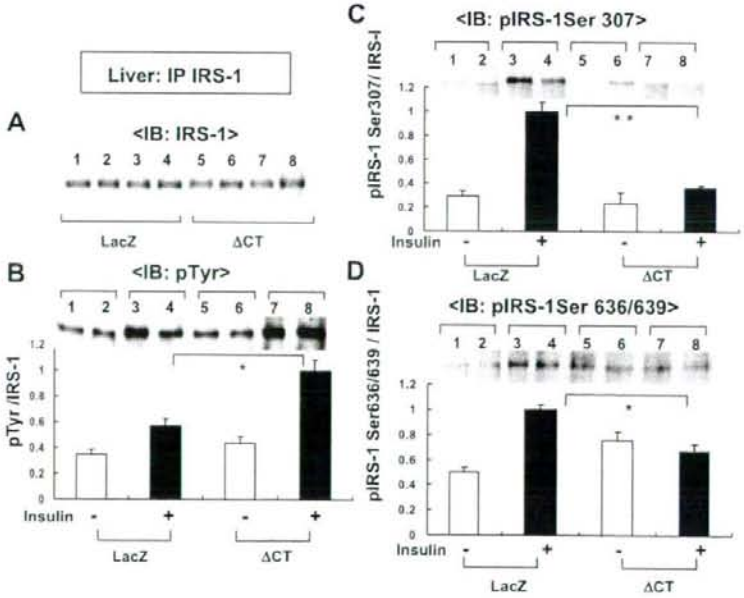

Fig. 5. Insulin-induced IRS-1 tyrosine residue and Ser^{307} and $Ser^{636/639}$ phosphorylations in hepatic raptor-ΔC_T mice. Four days after adenovirus injection the livers were removed after insulin or saline administration, followed by immunoprecipitation (IP) with IRS-1 antibody. SDS-PAGE and IB were then performed using the appropriate antibody as a probe. *A*: there was no difference between raptor-ΔC_T and control mice in the expression of IRS-1 protein. *B*: insulin-induced IRS-1 tyrosine phosphorylation was significantly increased in raptor-ΔC_T mice. *C* and *D*: insulin-induced IRS-1 Ser^{307} and $Ser^{636/639}$ phosphorylations were markedly depressed in raptor-ΔC_T mice. LacZ: $n = 8$ (insulin$^+$: $n = 4$; insulin$^-$: $n = 4$); ΔC_T: $n = 8$ (insulin$^+$: $n = 4$; insulin$^-$: $n = 4$). $^*P < 0.05$, $^{**}P < 0.01$.

differences in hepatic expression levels of IRS-1 protein between raptor-ΔC_T and control mice. Insulin-induced IRS-1 tyrosine phosphorylation was significantly increased in hepatic raptor-ΔC_T-overexpressing mice (Fig. 5*B*), whereas insulin-induced IRS-1 Ser^{307} and $Ser^{636/639}$ phosphorylation were markedly depressed in raptor-ΔC_T mice (Fig. 5, *C* and *D*). Moreover, we performed PI 3-kinase assays of the liver to investigate PI 3-kinase activity. Figure 6 presents insulin-induced tyrosine phosphorylation-associated PI 3-kinase activity and IRS-1-associated PI 3-kinase activity, both of which were increased approximately twofold compared with those of LacZ mice. Insulin-induced Akt Ser^{473} and Thr^{308} phosphorylations were markedly increased in raptor-ΔC_T mice (Fig. 7, *B* and *C*), as shown by immunoblotting of liver lysates with Akt and phospho-Akt Ser^{473} and Thr^{308} antibodies, but there was no difference between these mice in Akt protein expression (Fig. 7*A*). In addition, basal Akt Ser^{473} and Thr^{308} phosphorylations were also markedly increased in raptor-ΔC_T mice (Fig. 7, *B* and *C*).

DISCUSSION

Insulin resistance is induced by many factors, including obesity, high-fat diet, insufficient exercise, hypertension (13), and various hormones. Among these factors, obesity induced by excessive caloric intake is considered to be the most common and important factor leading to the occurrence of diabetes mellitus. In obese animals, PI 3-kinase activation via the association with IRS proteins is impaired, and increased serine phosphorylation in IRS-1 is reportedly involved in this impaired insulin-induced PI 3-kinase activation. Phosphorylation of serine residues of IRS-1 is also reportedly involved in IRS-1 degradation (1, 18, 25). To date, several serine/threonine kinases have been reported to phosphorylate serine residues of IRS-1.

IRS-1 phosphorylation mechanisms under insulin-resistant conditions can essentially be divided into two major categories. One involves adipocyte-derived factors such as TNFα, resistin, and free fatty acids, which activate JNK and/or ERK and thereby increase the serine phosphorylation of IRS-1. The other operates in response to intracellular nutrient conditions. The nutritional status of the cell directly regulates the AMPK/mTOR pathway independently of proteins secreted by adipocytes, and mTOR and S6K reportedly enhance phosphorylation

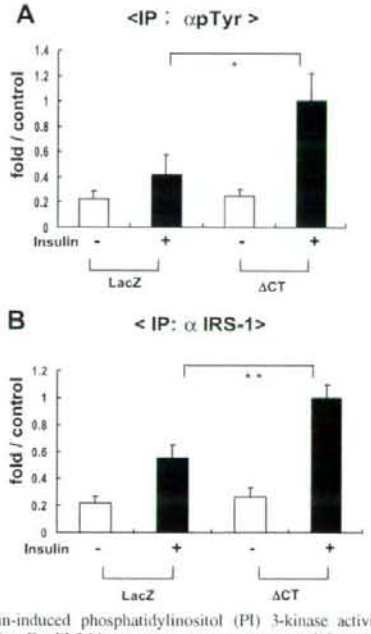

Fig. 6. Insulin-induced phosphatidylinositol (PI) 3-kinase activity in hepatic raptor-ΔC_T mice. For PI 3-kinase assay, supernatants containing equal amounts of protein were immunoprecipitated for 2 h at 4°C with anti-IRS-1 or phosphorylated tyrosine antibody and protein A- or G-Sepharose. PI 3-kinase activities in the immunoprecipitates were assayed. *A* and *B*: insulin-induced, tyrosine phosphorylation-associated PI 3-kinase activity and IRS-1-associated PI 3-kinase activity were both increased to approximately double those of LacZ mice. LacZ: $n = 8$ (insulin$^+$: $n = 4$; insulin$^-$: $n = 4$); ΔC_T: $n = 8$ (insulin$^+$: $n = 4$; insulin$^-$: $n = 4$). $^*P < 0.05$; $^{**}P < 0.01$.

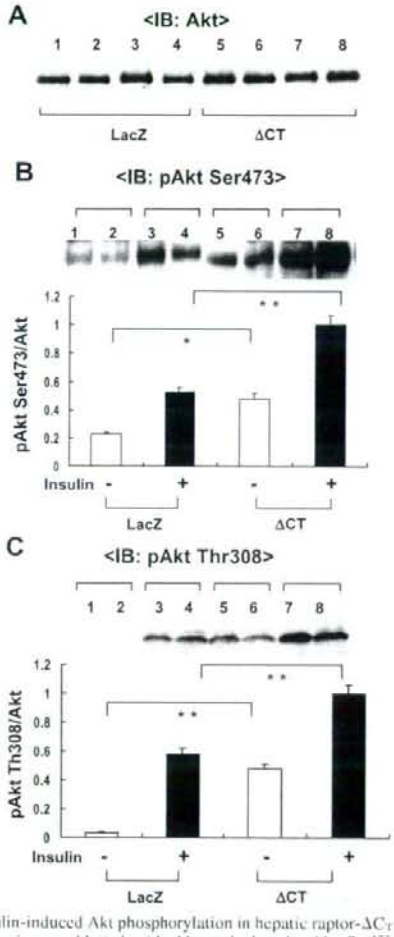

Fig. 7. Insulin-induced Akt phosphorylation in hepatic raptor-ΔC_T mice. Liver lysates were immunoblotted with Akt and phospho-Akt Ser^{473} and Thr^{308} antibody. *A*: there was no difference in Akt protein expression levels between these mice. *B* and *C*: basal Akt Ser^{473} and Thr^{308} phosphorylation as well as insulin-induced Akt Ser^{473} and Thr^{308} phosphorylation were also markedly increased in raptor-ΔC_T mice. LacZ: $n = 8$ (insulin$^+$: $n = 4$; insulin$^-$: $n = 4$); ΔC_T: $n = 8$ (insulin$^+$: $n = 4$; insulin$^-$: $n = 4$). $^*P < 0.05$; $^{**}P < 0.01$.

of serine residues of IRS-1 (3, 5, 16). Although S6K1-deficient mice were shown to be resistant to age- and diet-induced obesity and insulin resistance (26), we investigated the acute effect of transient inhibition of raptor on the impaired insulin signaling and glucose intolerance of K/KAy mice with genetic obesity-associated insulin resistance. In the K/KAy mice, one of the obese rodent models, IRS-1 Ser^{307} and IRS-1 $Ser^{636/639}$ phosphorylations are elevated (26).

Raptor contains a highly conserved amino-terminal domain, followed by several HEAT repeats and seven carboxy-terminal WD40 repeats (4), and acts as an adaptor to recruit substrates $p70^{S6k}$ and 4E-BP1 to mTOR (2, 12, 23). The domains in raptor and mTOR that interact with each other have been clearly demonstrated and suggest multiple contact sites between these two proteins (4, 10), in contrast with the selective binding of $p70^{S6k}$ to the NH_2-terminal portion of raptor (12). We were unable to detect the associations of raptor and COOH-terminally deleted raptor (raptor-ΔC_T) with endogenous S6K (data not shown). However, it was demonstrated that raptor-ΔC_T binds to a far smaller amount of mTOR but not to IRS-1, whereas wild-type raptor binds to both. Indeed, IRS-1 phosphorylation at $Ser^{636/639}$ was markedly decreased by raptor-ΔC_T overexpression. These findings suggest that raptor-ΔC_T functions as a dominant negative protein for mTOR/S6K or mTOR/IRS-1 signaling.

Interestingly, we found that 4E-BP1 phosphorylations of both $Thr^{37/46}$ and Thr^{70} in the liver were significantly increased by raptor-ΔC_T overexpression. Thus, the inhibitory effect of raptor-ΔC_T is specific for S6K. This result was unexpected, but it is hoped that it will provide useful information regarding how the raptor-mTOR complex recognizes individual downstream molecules. We speculate that S6K, but not 4E-BP1, preferentially associates with raptor-ΔC_T to full-length raptor. If so, raptor-ΔC_T overexpression would inhibit S6K binding, but not that of 4E-BP1, with the mTOR/raptor complex. It is also possible that some unidentified molecule is required for this association between S6K and the raptor-mTOR complex and that raptor-ΔC_T binds to this as yet unknown molecule. In this case, S6K cannot bind the mTOR complex in the raptor-ΔC_T-overexpressing cells, whereas 4E-BP1 phosphorylated is unaffected. Further study is necessary to resolve this issue.

In the present study, hepatic overexpression of raptor-ΔC_T strongly inhibited insulin-induced $p70^{S6k}$ activation and improved glucose intolerance and hyperinsulinemia. Importantly, Akt phosphorylation was markedly enhanced not only under insulin-stimulated but also basal conditions. Decreased IRS-1 Ser^{307} and $Ser^{636/639}$ phosphorylations and the resulting increases in tyrosine phosphorylation of IRS-1 and subsequent PI 3-kinase activity can account for the increased Akt phosphorylation under insulin-stimulated conditions. However, this may not fully explain the mechanism leading to markedly increased basal Akt phosphorylation since basal PI 3-kinase activity was not altered by raptor-ΔC_T. Thus, it is possible that other mechanisms, such as increased PDK and/or rictor activity, or even suppression of Akt dephosphorylation, are involved in the increased basal Akt phosphorylation. Indeed, it has been reported (22) that raptor-mTOR and rictor-mTOR complexes regulate Akt phosphorylation in a reverse manner. Further study is necessary to clarify whether suppression of the raptor-mTOR complex via overexpression of raptor-ΔC_T leads to elevated rictor-mTOR activity or suppressed Akt dephosphorylation.

In summary, we demonstrated that hepatic $p70^{S6k}$ inhibition in diabetic mice improves glucose tolerance by enhancing both basal and insulin-stimulated Akt phosphorylations. Although further experiments are needed to clarify the molecular mechanisms of increased basal Akt phosphorylation, our results suggest that mTORC1 inhibition is a potential treatment strategy for obesity-related insulin resistance.

REFERENCES

1. **Carvalho E, Jansson PA, Axelsen M, Eriksson JW, Huang X, Groop L, Rondinone C, Sjostrom L, Smith U.** Low cellular IRS 1 gene and protein expression predict insulin resistance and NIDDM. *FASEB J* 13: 2173–2178, 1999.
2. **Choi KM, McMahon LP, Lawrence JC Jr.** Two motifs in the translational repressor PHAS-I required for efficient phosphorylation by mammalian target of rapamycin and for recognition by raptor. *J Biol Chem* 278: 19667–19673, 2003.
3. **Dennis PB, Jaeschke A, Saitoh M, Fowler B, Kozma SC, Thomas G.** Mammalian TOR: a homeostatic ATP sensor. *Science* 294: 1102–1105, 2001.
4. **Hara K, Maruki Y, Long X, Yoshino K, Oshiro N, Hidayat S, Tokunaga C, Avruch J, Yonezawa K.** Raptor, a binding partner of target of rapamycin (TOR), mediates TOR action. *Cell* 110: 177–189, 2002.
5. **Hara K, Yonezawa K, Weng QP, Kozlowski MT, Belham C, Avruch J.** Amino acid sufficiency and mTOR regulate p70 S6 kinase and eIF-4E BP1 through a common effector mechanism. *J Biol Chem* 273: 14484–14494, 1998.
6. **Harrington LS, Findlay GM, Gray A, Tolkacheva T, Wigfield S, Rebholz H, Barnett J, Leslie NR, Cheng S, Shepherd PR, Gout I, Downes CP, Lamb RF.** The TSC1–2 tumor suppressor controls insulin-PI3K signaling via regulation of IRS proteins. *J Cell Biol* 166: 213–223, 2004.
7. **Hay N, Sonenberg N.** Upstream and downstream of mTOR. *Genes Dev* 18: 1926–1945, 2004.
8. **Hirosumi J, Tuncman G, Chang L, Gorgun CZ, Uysal KT, Maeda K, Karin M, Hotamisligil GS.** A central role for JNK in obesity and insulin resistance. *Nature* 420: 333–336, 2002.
9. **Jacinto E, Loewith R, Schmidt A, Lin S, Ruegg MA, Hall A, Hall MN.** Mammalian TOR complex 2 controls the actin cytoskeleton and is rapamycin insensitive. *Nat Cell Biol* 6: 1122–1128, 2004.
10. **Kim DH, Sarbassov DD, Ali SM, King JE, Latek RR, Erdjument-Bromage H, Tempst P, Sabatini DM.** mTOR interacts with raptor to form a nutrient-sensitive complex that signals to the cell growth machinery. *Cell* 110: 163–175, 2002.
11. **Kushiyama A, Shojima N, Ogihara T, Inukai K, Sakoda H, Fujishiro M, Fukushima Y, Anai M, Ono H, Horike N, Viana AY, Uchijima Y, Nishiyama K, Shimosawa T, Fujita T, Katagiri H, Oka Y, Kurihara H, Asano T.** Resistin-like molecule beta activates MAPKs, suppresses insulin signaling in hepatocytes, and induces diabetes, hyperlipidemia, and fatty liver in transgenic mice on a high fat diet. *J Biol Chem* 280: 42016–42025, 2005.
12. **Nojima H, Tokunaga C, Eguchi S, Oshiro N, Hidayat S, Yoshino K, Hara K, Tanaka N, Avruch J, Yonezawa K.** The mammalian target of rapamycin (mTOR) partner, raptor, binds the mTOR substrates p70 S6 kinase and 4E-BP1 through their TOR signaling (TOS) motif. *J Biol Chem* 278: 15461–15464, 2003.
13. **Ogihara T, Asano T, Fujita T.** Contribution of salt intake to insulin resistance associated with hypertension. *Life Sci* 73: 509–523, 2003.
14. **Ogihara T, Asano T, Katagiri H, Sakoda H, Anai M, Shojima N, Ono H, Fujishiro M, Kushiyama A, Fukushima Y, Kikuchi M, Noguchi N, Aburatani H, Gotoh Y, Komuro I, Fujita T.** Oxidative stress induces insulin resistance by activating the nuclear factor-kappa B pathway and disrupting normal subcellular distribution of phosphatidylinositol 3-kinase. *Diabetologia* 47: 794–805, 2004.
15. **Ogihara T, Shin BC, Anai M, Katagiri H, Inukai K, Funaki M, Fukushima Y, Ishihara H, Takata K, Kikuchi M, Yazaki Y, Oka Y, Asano T.** Insulin receptor substrate (IRS)-2 is dephosphorylated more rapidly than IRS-1 via its association with phosphatidylinositol 3-kinase in skeletal muscle cells. *J Biol Chem* 272: 12868–12873, 1997.

16. **Patti ME, Brambilla E, Luzi L, Landaker EJ, Kahn CR.** Bidirectional modulation of insulin action by amino acids. *J Clin Invest* 101: 1519–1529, 1998.
17. **Pende M, Kozma SC, Jaquet M, Oorschot V, Burcelin R, Le Marchand-Brustel Y, Klumperman J, Thorens B, Thomas G.** Hypoinsulinaemia, glucose intolerance and diminished beta-cell size in S6K1-deficient mice. *Nature* 408: 994–997, 2000.
18. **Pirola L, Bonnafous S, Johnston AM, Chaussade C, Portis F, Van Obberghen E.** Phosphoinositide 3-kinase-mediated reduction of insulin receptor substrate-1/2 protein expression via different mechanisms contributes to the insulin-induced desensitization of its signaling pathways in L6 muscle cells. *J Biol Chem* 278: 15641–15651, 2003.
19. **Sakoda H, Gotoh Y, Katagiri H, Kurokawa M, Ono H, Onishi Y, Anai M, Ogihara T, Fujishiro M, Fukushima Y, Abe M, Shojima N, Kikuchi M, Oka Y, Hirai H, Asano T.** Differing roles of Akt and serum- and glucocorticoid-regulated kinase in glucose metabolism, DNA synthesis, and oncogenic activity. *J Biol Chem* 278: 25802–25807, 2003.
20. **Sarbassov DD, Ali SM, Kim DH, Guertin DA, Latek RR, Erdjument-Bromage H, Tempst P, Sabatini DM.** Rictor, a novel binding partner of mTOR, defines a rapamycin-insensitive and raptor-independent pathway that regulates the cytoskeleton. *Curr Biol* 14: 1296–1302, 2004.
21. **Sarbassov DD, Ali SM, Sabatini DM.** Growing roles for the mTOR pathway. *Curr Opin Cell Biol* 17: 596–603, 2005.
22. **Sarbassov DD, Guertin DA, Ali SM, Sabatini DM.** Phosphorylation and regulation of Akt/PKB by the rictor-mTOR complex. *Science* 307: 1098–1101, 2005.
23. **Schalm SS, Fingar DC, Sabatini DM, Blenis J.** TOS motif-mediated raptor binding regulates 4E-BP1 multisite phosphorylation and function. *Curr Biol* 13: 797–806, 2003.
24. **Shah OJ, Wang Z, Hunter T.** Inappropriate activation of the TSC/Rheb/mTOR/S6K cassette induces IRS1/2 depletion, insulin resistance, and cell survival deficiencies. *Curr Biol* 14: 1650–1656, 2004.
25. **Tzatsos A, Kandror KV.** Nutrients suppress phosphatidylinositol 3-kinase/Akt signaling via raptor-dependent mTOR-mediated insulin receptor substrate 1 phosphorylation. *Mol Cell Biol* 26: 63–76, 2006.
26. **Um SH, Frigerio F, Watanabe M, Picard F, Joaquin M, Sticker M, Fumagalli S, Allegrini PR, Kozma SC, Auwerx J, Thomas G.** Absence of S6K1 protects against age- and diet-induced obesity while enhancing insulin sensitivity. *Nature* 431: 200–205, 2004.
27. **Wullschleger S, Loewith R, Hall MN.** TOR signaling in growth and metabolism. *Cell* 124: 471–484, 2006.

Am J Physiol Renal Physiol 294: F542–F553, 2008.
First published January 2, 2008; doi:10.1152/ajprenal.00201.2007.

Multiple renal cysts, urinary concentration defects, and pulmonary emphysematous changes in mice lacking TAZ

Ryosuke Makita,[1,2] Yasunobu Uchijima,[1] Koichi Nishiyama,[1] Tomokazu Amano,[2] Qin Chen,[3] Takumi Takeuchi,[3] Akihisa Mitani,[1,4] Takahide Nagase,[4] Yutaka Yatomi,[5] Hiroyuki Aburatani,[6] Osamu Nakagawa,[7,8] Erin V. Small,[7] Patricia Cobo-Stark,[9] Peter Igarashi,[9] Masao Murakami,[1,10] Junji Tominaga,[1] Takahiro Sato,[1] Tomoichiro Asano,[1,11] Yukiko Kurihara,[1] and Hiroki Kurihara[1]

Departments of [1]Physiological Chemistry and Metabolism, [2]Developmental Medical Technology (Sankyo), [3]Urology, [4]Respiratory Medicine, and [5]Laboratory Medicine, Graduate School of Medicine and [6]Genome Science Division, Research Center for Advanced Science and Technology, The University of Tokyo, Tokyo; [10]Department of Medicine and Clinical Science, Kyoto University Graduate School of Medicine, Kyoto; [11]Department of Biomedical Chemistry, Hiroshima University Graduate School of Biomedical Sciences, Hiroshima, Japan; and [7]Division of Cardiology, Departments of Internal Medicine, [8]Molecular Biology, and [9]Internal Medicine and Pediatrics, The University of Texas Southwestern Medical Center at Dallas, Dallas, Texas

Submitted 28 April 2007; accepted in final form 31 December 2007

Makita R, Uchijima Y, Nishiyama K, Amano T, Chen Q, Takeuchi T, Mitani A, Nagase T, Yatomi Y, Aburatani H, Nakagawa O, Small EV, Cobo-Stark P, Igarashi P, Murakami M, Tominaga J, Sato T, Asano T, Kurihara Y, Kurihara H. Multiple renal cysts, urinary concentration defects, and pulmonary emphysematous changes in mice lacking TAZ. *Am J Physiol Renal Physiol* 294: F542–F553, 2008. First published January 2, 2008; doi:10.1152/ajprenal.00201.2007.— TAZ (transcriptional coactivator with PDZ-binding motif), also called WWTR1 (WW domain containing transcription regulator 1), is a 14-3-3-binding molecule homologous to Yes-associated protein. TAZ acts as a coactivator for several transcription factors as well as a modulator of membrane-associated PDZ domain-containing proteins, but its (patho)physiological roles remain unknown. Here we show that gene inactivation of TAZ in mice resulted in pathological changes in the kidney and lung that resemble the common human diseases polycystic kidney disease and pulmonary emphysema. *Taz*-null/*lacZ* knockin mutant homozygotes demonstrated renal cyst formation as early as *embryonic day 15.5* with dilatation of Bowman's capsules and proximal tubules, followed by pelvic dilatation and hydronephrosis. After birth, only one-fifth of TAZ-deficient homozygotes grew to adulthood and demonstrated multicystic kidneys with severe urinary concentrating defects and polyuria. Furthermore, adult TAZ-deficient homozygotes exhibited diffuse emphysematous changes in the lung. Thus TAZ is essential for developmental mechanisms involved in kidney and lung organogenesis, whose disturbance may lead to the pathogenesis of common human diseases.

renal disease; knockout mice; transcription factor

TAZ (TRANSCRIPTIONAL COACTIVATOR with PDZ-binding motif), also called WWTR1 (WW domain containing transcription regulator 1), is a 14-3-3-binding molecule homologous to Yes-associated protein (YAP) (14, 18). TAZ, as well as YAP, possess a WW domain that can bind to the PPXY motif present in some transcription factors. Through this interaction and additional unknown mechanisms, TAZ can act as a coactivator for several transcription factors, including Runx2/Cbfa1, TTF-1/Nkx2.1, Tbx5, and Pax3 (5, 24, 25, 30). The COOH-terminal region of TAZ contains a PSD-95, Dlg, and ZO-1 homology (PDZ)-binding motif that localizes TAZ to discrete foci in the nucleus and is essential for its activity as a transcriptional coactivator (18). TAZ and YAP also bind to membrane-associated PDZ domain-containing proteins through this motif. In particular, TAZ and YAP bind to sodium/hydrogen exchanger regulatory factor (NHERF)-2 and NHERF, respectively, which may link TAZ and YAP to transmembrane receptors and actin-binding proteins (14, 18). Furthermore, a recent report demonstrated that TAZ may modulate mesenchymal stem cell differentiation into osteogenic and adipogenic lineages by coactivating Runx2/Cbfa1 and repressing peroxisome proliferator-activated receptor-γ-dependent gene transcription (13). Thus TAZ and YAP are now regarded as context-dependent transcriptional modulators in various cell types that may link events at the plasma membrane and cytoskeleton to nuclear transcription, possibly in a 14-3-3-dependent manner (14, 18).

In midgestation mouse embryos, TAZ is mainly expressed in the paraxial mesoderm, limb buds, and the neural tube (25). Later, TAZ is distributed more broadly in various tissues and organs (18 and UniGene's EST ProfileViewer). The broad distribution of TAZ and its interaction with different transcription factors essential for embryonic development led us to investigate the physiological role of TAZ by a gene targeting strategy.

Here, we demonstrate that inactivation of the mouse *Taz* gene in mice results in the formation of multiple cysts in the kidney and greatly enlarged air spaces in the lung. These phenotypes resemble human polycystic kidney diseases (PKD) and pulmonary emphysema, respectively. PKD is a human inherited renal disorder that is the most common genetic cause of renal failure in children and adults (3, 15). Autosomal dominant polycystic kidney disease (ADPKD) is the most prevalent form, with an incidence of 1–2 per 1,000 individuals and is characterized by bilateral formation of multiple cysts arising from any segment of the nephrons and collecting ducts. ADPKD is caused by mutations in either of two genes, *PKD1*

Address for reprint requests and other correspondence: H. Kurihara, Dept. of Physiological Chemistry and Metabolism, Graduate School of Medicine, Univ. of Tokyo, 7-3-1 Hongo, Bunkyo-ku, Tokyo 113-0033, Japan (e-mail: kuri-tky@umin.ac.jp).

The costs of publication of this article were defrayed in part by the payment of page charges. The article must therefore be hereby marked "*advertisement*" in accordance with 18 U.S.C. Section 1734 solely to indicate this fact.

and *PKD2*, that encode membrane-associated proteins polycystin-1 and polycystin-2, respectively (23, 32, 33). Autosomal recessive polycystic kidney disease (ARPKD) is much less frequent (1/20,000 live births) and is caused by mutations of *PKHD1* (29, 37), which encodes polyductin/fibrocystin, a large transmembrane protein. Although the causative genes have been identified, the molecular mechanism underlying cystic formation remains largely unknown.

TAZ-deficient mice also exhibited urinary concentration defects, polyuria, and hydronephrosis. Although urinary concentrating defects have been observed in human ADPKD and ARPKD, massive polyuria and hydronephrosis are uncommon. These findings suggest that the pathophysiological processes in TAZ-deficient kidneys and human PKD are different in some respects. The similarities and dissimilarities between TAZ-deficient mice and PKD may provide important clues to understanding the pathogenesis of a common human disease.

In addition, the dilatation of air spaces of the lung in TAZ-deficient mice is morphologically reminiscent of human pulmonary emphysema, which is a common disease that causes death and disability, especially in the aged (1, 12). As a manifestation of chronic obstructive pulmonary disease (COPD), pulmonary emphysema is characterized by enlargement of air spaces and destruction of the alveolar wall. Although α-antitrypsin deficiency is known to cause a congenital form of pulmonary emphysema, little remains known concerning the molecular mechanisms underlying the pathogenesis of this disease. TAZ-deficient mice may also serve as a novel animal model for COPD as well as kidney diseases.

MATERIALS AND METHODS

Generation and genotyping of mutant mice. A C57BL6/J-derived BAC clone containing the mouse *Taz* gene was obtained from BACPAC Resource Center (Oakland, CA). The *nls-lacZ/PGKneo* cassette was made by placing the *lacZ* gene with a nuclear localization signal (*nls-lacZ*) adjacent to the *PGKneo* gene and flanking it with *lox71* at the 5′-end and *lox2272* at the 3′-end to allow recombinase-mediated cassette exchange. A pKO Scrambler NTKV-1904 plasmid (Stratagene) was used as a backbone vector. For the targeting construct, a PCR-amplified 1.2-kb fragment extending from the promoter region to the 5′-untranslated region in exon 2 and an 8.2-kb *Ngo*MIV-*Bam*HI fragment from intron 2 were inserted on each side of the *nls-lacZ/PGKneo* cassette (Fig. 1*A*). The targeting vector was linearized and electroporated into the B6129F1-derived embryonic stem (ES) cell line ATOM1 (Amano T et al., unpublished observations).

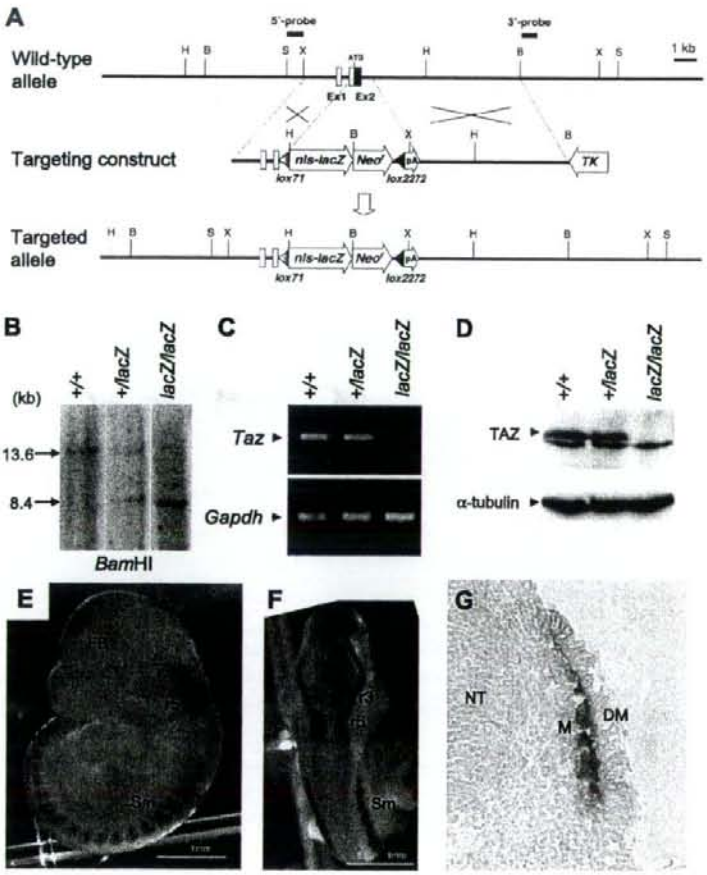

Fig. 1. Targeting of the mouse *Taz* (transcriptional coactivator with PDZ-binding motif) gene. *A*: schematic representation of the targeting strategy employed to knockin an *nls-lacZ* cassette into the *Taz* locus. Two different probes for genotyping are indicated as 5′- and 3′-probes. B, *Bam*HI; H, *Hind*III; S, *Sful*; X, *Xba*I. *B*: representative genotyping of the offspring from an F_1 intercross by Southern blot analysis. Genomic DNA samples were digested with *Bam*HI and probed with the 5′-probe. Bands of 13.6 and 8.4 kb represent wild-type and mutant alleles, respectively. *C* and *D*: RT-PCR (*C*) and Western blot (*D*) confirming the absence of TAZ expression in $Taz^{lacZ/lacZ}$ embryos. Total RNA and protein extracts were obtained from *embryonic day 15.5* whole embryos. Lower band in *D*, *top*, represents nonspecific binding. *E–G*: lateral (*E*) and dorsal (*F*) views of an *embryonic day 9.5* $Taz^{+/lacZ}$ embryo and a section at the level of the somites (*G*) stained with X-gal. FB, forebrain; DM, dermomyotome; M, myotome; NT, neural tube; r3 and r5, rhombomeres 3 and 5 of the hindbrain; Sm, somites.

Clones that survived positive-negative selection with neomycin and 1-(2'-deoxy-2'-fluoro-1-β-D-arabinofuranosyl)-5-iodouracil were screened for homologous recombination with diagnostic PCR primers. Targeted clones were injected in ICR blastocysts to generate germline chimeras. Mice homozygous for the *Taz*^{lacZ} allele were obtained by intercrossing F_1 heterozygotes. The genotypes of the offspring were determined by PCR or Southern blot analysis on tail-tip or amnion DNA. All animal experiments were reviewed and approved by the University of Tokyo Animal Care and Use Committee.

RT-PCR. Total RNA was extracted using ISOGEN (Nippon Gene). The reverse transcription reaction was carried out using SuperScriptIII (Invitrogen). PCR was then performed on the resulting cDNA using the primers 5'-GAAAATCACCACATGGCAAGACCC-3' and 5'-TTACAGCCAGGTTAGAAAGGGCTC-3' for *TAZ* (product size, 748 bp; annealing, 64°C), 5'-GGCTATGTGCAGTGTCATGTC-3' and 5'-CTGTGATATGCCAGTGGTCAG-3' for *Aqp1* (product size, 462 bp; annealing, 58°C), 5'-TGGATTCATGGAGCAGCCCGGT-3' and 5'-TCCTTCCTTCGAGCTGCCTTC-3' for*Aqp2* (product size, 312 bp; annealing, 58°C), 5'-ATCAAGCTGCCCATCTACAC-3' and 5'-GGGCCAGCTTCACATTCTC-3' for *Aqp3* (product size, 559 bp; annealing, 56°C), and 5'-GGTGTGAACCACGAGAAATAT-3' and 5'-AGATCCACGACGGACACATT-3' for *Gapdh* (product size, 335 bp; annealing, 56°C). For comparison of *Pkd1*, *Pkd2*, and *Pkhd1* expression levels, quantitative real-time RT-PCR was performed using the LightCycler system (Roche diagnostics) according to the manufacturer's protocol. Sequences of the primers were as follows; 5'-GGATGGTGATCAGACACCGCTCAA-3' and 5'-TTGGTGGCTTCTTCCTTCCGACCT-3' for *Pkd1*, 5'-TCTCCTCAGGTTATTGGCGGAGTT-3' and 5'-GACATAGCGGATCAGTTTTACAGG-3' for *Pkd2*, 5'-GGCGCCACAGACAAACAATTA-3' and 5'-GCCCTGCAGTTCTAGCTTGGTT-3' for *Pkhd1*, and 5'-GGTTGGCCCTGGGAGTACCAAGAA-3' and 5'-AATGGGAAGCCCAAGTGCCTCTGT-3' for *Avpr2*.

Western blotting. Anti-TAZ rabbit polyclonal antibody was previously described (25). Western blotting was performed on lysates from *embryonic day 13.5* whole embryos or 12-wk-old kidneys using a standard protocol.

Histology. For histological analysis, samples were fixed in formalin, embedded in paraffin, cut into 2-μm-thick sections, and stained with hematoxylin and eosin. Photomicrographs were obtained using a computer-assisted microscope (Nikon ECLIPSE 80i).

Urinary analysis. Urine volume was measured using the 48-h frequency/volume analysis system as previously described (4). Briefly, each mouse was placed in a metabolic cage connected to a digital scale and personal computer. Each mouse was provided with free access to food and water. After mice were acclimatized for 2 days in the cage, water intake, urine voiding frequency, and volume per void were recorded for 48 h.

Lectin and immunofluorescent staining. Lectin staining was performed on cryosectioned kidneys. *Embryonic day 18.5* kidneys were dissected, embedded in optimum-cutting temperature (OCT) compound (Miles), and cut into 10-μm-thick sections. After being blocked with blocking buffer, the sections were incubated for 1 h at 37°C with 20 μg/ml biotin-conjugated *Dolichos biflorus* agglutinin (DBA) or *Lotus tetragonolobus* agglutinin (LTA) followed by extensive washing with blocking buffer. Lectin staining was visualized by reacting with fluorescein isothiocyanate-conjugated streptavidin, and nuclei were counterstained with propidium iodide. Photomicrographs were obtained using a computer-assisted confocal microscope (Nikon D-ECLIPSE C1).

For immunofluorescent staining, paraformaldehyde-fixed cryosections were stained with antibodies to aquaporin-2 (gift from M. Knepper, National Heart, Lung, and Blood Institute, Bethesda, MD) or aquaporin-3 (Chemicon), as described previously (31). Nuclei were stained with 4',6-diamidine-2-phenylindole (DAPI).

In situ hybridization. Isotopic in situ hybridization was performed on paraffin-embedded sections of *embryonic day 14.5* and *16.5* embryos using ^{35}S-radiolabeled RNA probes for *Taz/Wwtr1* as previously described (27).

β-Galactosidase staining. LacZ expression was detected by staining with X-gal (5-bromo-4-chloro-3-indoyl β-D-galactoside). Staining was performed as described by Nagy et al. (26) with minor modifications. Whole embryos and kidneys were washed in ice-cold PBS containing 2 mM $MgCl_2$ and fixed in 0.1 M phosphate buffer (pH 7.3) containing 0.2% glutaraldehyde, 5 mM EGTA, and 2 mM $MgCl_2$. Following rinsing three times with 0.1 M phosphate buffer containing 2 mM $MgCl_2$, 0.02% Nonidet P-40, 0.01% sodium deoxycholate, and 5 mM EGTA (washing buffer), samples were embedded in OCT compound and cryosectioned. Embryos or sections were incubated overnight at 37°C in X-gal-staining buffer (10 mM potassium ferrocyanide, 10 mM potassium ferricyanide and 2 mg/ml X-gal in washing buffer). For costaining with platelet/endothelial cell adhesion molecule, X-gal-stained sections were rinsed with PBS, incubated in the blocking buffer (see *Lectin and immunofluorescent staining*), and reacted with anti-CD31 antibody (BD Bioscience) (1:100) at 4°C overnight. Immunoreactivity was visualized with the VECTASTAIN ABC kit (Vector laboratories). Sections were counterstained with 1% Orange G (Sigma).

Morphometric analysis. The mean linear intercept, as a measure of interalveolar wall distance, was determined as described by Thurlbeck (34). Briefly, lines were drawn across light microscopic images of the lung section stained with hematoxylin and eosin. The mean linear intercept was calculated by dividing the total length of a line by the total number of intercepts encountered in 72 lines/lung.

Statistical analysis. Mann-Whitney nonparametric test was used to compare values between two groups for morphometric analysis. Student's *t*-test was used for the comparison of values in other experiments. Data were represented as means ± SD. Values of $P < 0.05$ were considered significant.

RESULTS

Generation of Taz-lacZ knockin mice. We disrupted the mouse *Taz* locus by replacing the coding region in exon 2 with an *nls-lacZ/PGKneo* cassette (Fig. 1*A*). Of 683 ES cell clones screened, three clones were positive for the mutant *Taz*^{lacZ} allele. All three clones were injected in ICR blastocysts and gave rise to male germline chimeras, which were subsequently bred with ICR females to produce *Taz*$^{+/lacZ}$ heterozygous mice. The heterozygous mice appeared normal and were fertile. Offspring from *Taz*$^{+/lacZ}$ intercrosses were genotyped by Southern analysis of tail genomic DNA (Fig. 1*B*). The absence of *Taz* transcripts and protein in *Taz*$^{lacZ/lacZ}$ homozygous mice was confirmed by RT-PCR and Western blotting, respectively (Fig. 1, *C* and *D*).

To verify that *Taz*-directed *lacZ* expression reflected the pattern of authentic *Taz* expression, we stained for *lacZ* in

Table 1. *Genotypic distribution of offspring from heterozygous matings*

Age	Wild-type	*Taz*$^{lacZ/+}$	*Taz*$^{lacZ/lacZ}$	Total
E8.5	8 (29)	12 (43)	8 (29)	28
E13.5	25 (19)	77 (58)	31 (23)	133
E15.5	52 (23)	114 (50)	61 (27)	227
E18.5	76 (27)	152 (53)	61 (21)	289
P0	31 (35)	45 (51)	12 (14)	88
P21	133 (33)	234 (59)	30 (8)	397

Nos. in parenthesis indicate percentage of the total numbers. E, embryonic day; P, day postpartum.

embryonic day 9.5 $Taz^{+/lacZ}$ embryos. At *embryonic day 9.5*, *lacZ* staining was observed in the somitic mesoderm and as in the neuroectoderm within the forebrain and hindbrain (Fig. 1, *E* and *F*). Within the somites, *lacZ* expression was detected in the myotome (Fig. 1*G*). These expression patterns coincide with that of authentic *Taz* expression revealed by in situ hybridization (25).

Early mortality in $Taz^{lacZ/lacZ}$ *mice.* When 309 littermates derived from $Taz^{+/lacZ}$ intercrosses were followed, 24 pups were found dead before 3 wk of age; 9 of 10 dead pups that could be genotyped were homozygous null. Genotyping of the remaining 285 littermates at 3 wk of age identified 90 wild-type (32%), 177 heterozygous (62%), and 18 homozygous (6%) mice, indicating that only one-fifth of the expected Mendelian ratio of $Taz^{lacZ/lacZ}$ mice were alive at weaning (Table 1).

To determine the stage at which homozygous null mice started to die, offspring from $Taz^{+/lacZ}$ intercrosses were genotyped at different embryonic stages. From *embryonic day 8.5* to *15.5*, the distribution of genotypes was close to the 1:2:1 Mendelian ratio (Table 1). At *embryonic day 18.5* and *day 0* postpartum, the numbers of $Taz^{lacZ/lacZ}$ homozygotes were lower than the expected ratio (Table 1), indicating that partial lethality started at the perinatal stage.

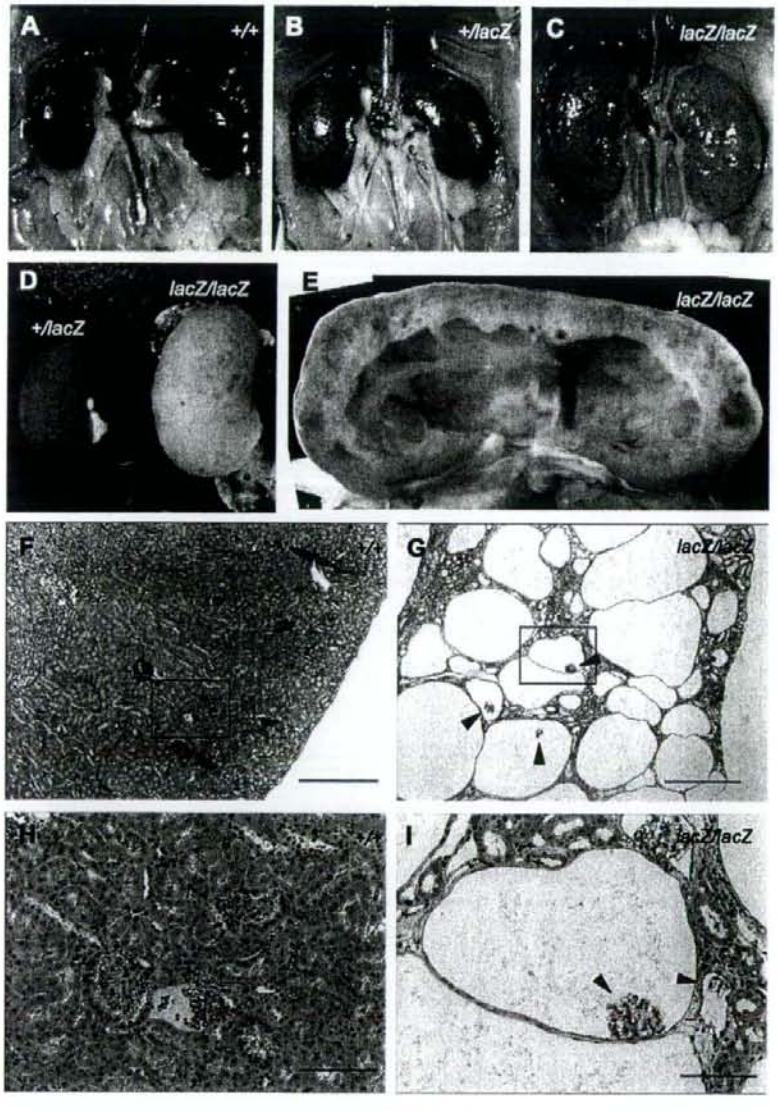

Fig. 2. Enlarged kidneys containing multiple cysts in $Taz^{lacZ/lacZ}$ mice. *A–C*: gross appearance of kidneys of $Taz^{+/+}$ (*A*), $Taz^{+/lacZ}$ (*B*), and $Taz^{lacZ/lacZ}$ (*C*) mice aged 10 wk. $Taz^{lacZ/lacZ}$ kidneys are enlarged, pale, and filled with numerous cysts. *D*: comparison of $TAZ^{+/lacZ}$ and $Taz^{lacZ/lacZ}$ kidneys. *E*: section of a $Taz^{lacZ/lacZ}$ kidney showing dilated calyx and thinned parenchyma containing multiple cysts. *F–I*: histology of $Taz^{+/+}$ (*F* and *H*) and $Taz^{lacZ/lacZ}$ (*G* and *I*) kidneys at low (*F* and *G*) and high (*H* and *I*) magnification. Boxed areas in *F* and *G* are magnified in *H* and *I*, respectively. $Taz^{lacZ/lacZ}$ kidneys exhibit numerous cysts of various sizes that are lined by a flattened epithelial monolayer. Cysts containing a glomerular tuft (arrowheads) are often observed. Scale bars indicate 500 μm (*F* and *G*) or 100 μm (*H* and *I*).

Multiple renal cysts and dilated calyces in $Taz^{lacZ/lacZ}$ mice. To characterize the phenotype that may be related to early mortality, we performed macroscopic and histological examinations on surviving $Taz^{lacZ/lacZ}$ mice. The most prominent abnormalities were first detected in the kidneys. Adult $Taz^{lacZ/lacZ}$ mice showed bilaterally enlarged, pale kidneys (Fig. 2, *C* and *D*). The calyces were extremely dilated, leaving thinned parenchyma containing multiple cysts (Fig. 2*E*). Histological analysis of 10-wk-old $Taz^{lacZ/lacZ}$ mice demonstrated numerous cysts of various sizes replacing most of the renal parenchyma (Fig. 2*G*), whereas no such changes were found in wild-type and $Taz^{+/lacZ}$ kidneys (Fig. 2, *F* and *H*). Cysts were lined by a flattened epithelial monolayer and sometimes contained a glomerular tuft, indicating an origin from Bowman's capsule (Fig. 2, *G* and *I*). The surrounding tissues showed increased interstitial fibrosis in Masson's trichrome staining (data not shown). Notably, these renal changes in $Taz^{lacZ/lacZ}$ mice shared a similar histology to human PKD.

In contrast, calyceal dilatation is uncommon in human PKD. To examine whether the dilation of the pelvis and atrophy of the medulla in $Taz^{lacZ/lacZ}$ kidneys could be secondary to anatomical obstruction in the urinary tract, we injected black ink into the pelvis of *embryonic day 18.5* kidneys. In $Taz^{lacZ/lacZ}$ kidneys, peristaltic passage of urine through the ureter was observed similar to wild-type and heterozygous littermates (data not shown). The urinary bladder was not apparently dilated in $Taz^{lacZ/lacZ}$ embryos at this stage (data not shown). These results suggested that the hydronephrotic changes in $Taz^{lacZ/lacZ}$ kidneys were not due to mechanical obstruction of the urinary tract.

Extrarenal phenotypes in $Taz^{lacZ/lacZ}$ mice. In human ADPKD, extrarenal manifestations are often observed in the liver, pancreas, blood vessels, heart, and other organs. However, examination of adult $Taz^{lacZ/lacZ}$ mice did not reveal obvious abnormalities in these tissues (data not shown). Instead, the lung was unexpectedly affected in $Taz^{lacZ/lacZ}$ mice. Histological examination revealed enlarged air spaces in $Taz^{lacZ/lacZ}$ lungs at the age of 8–9 mo (Fig. 3, *A* and *B*). The mean linear intercept, as a measure of interalveolar wall distance, was significantly greater in $Taz^{lacZ/lacZ}$ mice (149.6 ± 11.5 μm, $n = 4$) than in wild-type mice (51.6 ± 2.1 μm, $n = 4$) (Fig. 3*C*). There were no findings indicative of increased inflammation or fibrosis in $Taz^{lacZ/lacZ}$ lungs. The phenotype of $Taz^{lacZ/lacZ}$ lungs is highly reminiscent of human pulmonary emphysema.

The changes in the kidney and lung were observed in all the homozygous mice derived from two independent recombinant ES clones, although the severity of symptoms varied among individuals. In contrast, no wild-type and $Taz^{+/lacZ}$ mice displayed abnormalities (Figs. 2, *A* and *B*, and 3*A*).

Urinary concentration defects in $Taz^{lacZ/lacZ}$ mice. In addition to multiple cysts and dilated calyces, $Taz^{lacZ/lacZ}$ mice showed signs of polyuria. Indeed, the urinary bladder in $Taz^{lacZ/lacZ}$ mice was typically distended with a large volume of urine (data not shown). Measurement of the 48-h urine frequency and volume revealed that urine volume per void and total volume per day were much higher in $Taz^{lacZ/lacZ}$ mice than in $Taz^{+/lacZ}$ mice (Fig. 4). Measurements of urinary parameters showed polyuria and concentrating defects in $Taz^{lacZ/lacZ}$ mice, as indicated by lower urinary osmolality (Table 2). Overall electrolyte excretion was not enhanced, although excretion of chloride was slightly increased (Table 2), indicating that electrolyte reabsorption remained grossly preserved. Urinary albumin excretion in $Taz^{lacZ/lacZ}$ mice appeared to be increased, although the difference was not statistically significant (Table 2). The polyuria and concentrating defects in $Taz^{lacZ/lacZ}$ mice were not improved by vasopressin administration (data not shown), suggesting that the abnormalities were likely to be nephrogenic rather than due to vasopressin deficiency. Overall, $Taz^{lacZ/lacZ}$ kidneys were characterized by the concomitant occurrence of features that are typical of human PKD, including multicystic formation and urinary concentrating defects, and atypical features such as calyceal dilatation and hydronephrosis.

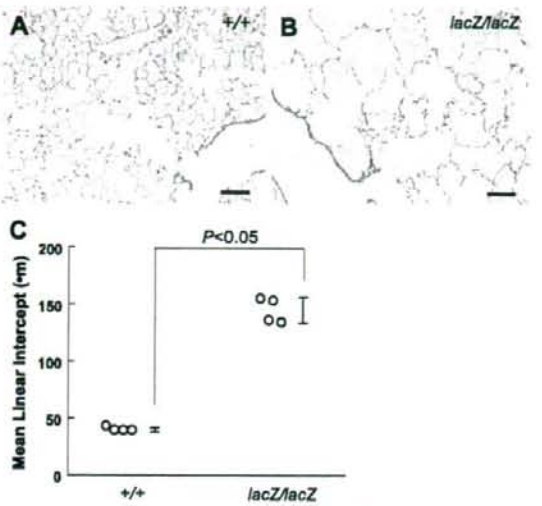

Fig. 3. Pulmonary emphysema-like changes in $Taz^{lacZ/lacZ}$ mice. *A* and *B*: hematoxylin and eosin staining of lung sections of $Taz^{+/+}$ (*A*) and $Taz^{lacZ/lacZ}$ (*B*) mice aged 9 mo. Enlarged air spaces and alveolar wall disruption are observed in the lung of $Taz^{lacZ/lacZ}$ mice. Scale bars indicate 100 μm. *C*: morphometric analysis. Mean linear intercept values are significantly greater in $Taz^{lacZ/lacZ}$ mice ($n = 4$) than wild-type mice ($n = 4$) aged 8–9 mo. A total of 288 lines drawn across the lung section were analyzed for each group. Error bars indicate SDs of the mean.

Cysts primarily originated from glomeruli and proximal tubules in $Taz^{lacZ/lacZ}$ embryos. To determine the time point at which cysts first arose in the kidneys of $Taz^{lacZ/lacZ}$ embryos, we performed histological analysis on kidneys at different embryonic stages. At *embryonic day 13.5*, the branching of ureteric buds and the initial formation of renal vesicles and comma- and S-shaped bodies appeared to be normal in both $Taz^{lacZ/lacZ}$ and wild-type kidneys (Fig. 5, *A* and *B*). At *embryonic day 15.5*, morphological abnormalities were first detected as dilatation of the Bowman's capsules and adjacent tubules in $Taz^{lacZ/lacZ}$ embryos (Fig. 5, *C* and *D*).

At *embryonic day 18.5*, $Taz^{lacZ/lacZ}$ kidneys exhibited tubules with varying degrees of dilatation and multiple cysts in inner cortical and medullary regions (Fig. 5, *E* and *F*). Cyst-lining epithelial cells appeared heterogeneous in morphology; some were flattened and others were rather cuboidal (Fig. 5, *G* and *H*). Glomerular tufts were detected in a small subset of cysts at this stage (Fig. 5, *G* and *H*). The renal pelvis was dilated, and the medulla was atrophic with disturbed formation of the papilla (Fig. 5, *E* and *F*). In contrast, the nephrogenic zone

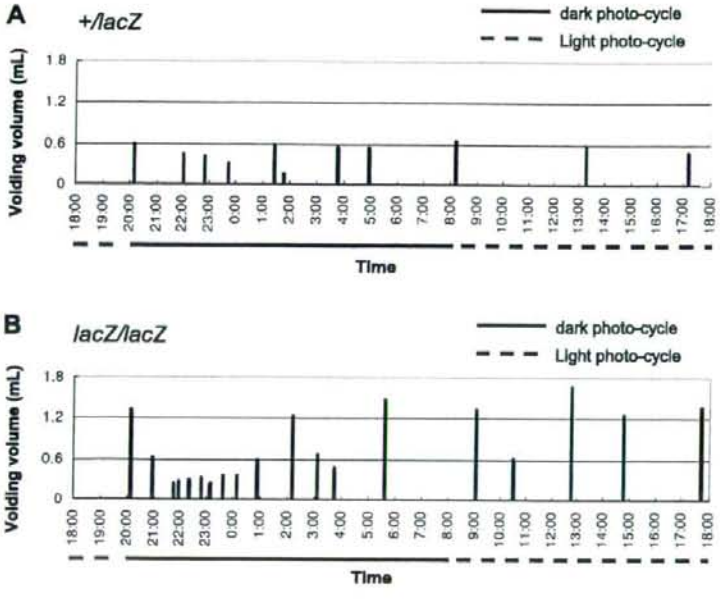

Fig. 4. Representative 24-h urinary frequency/volume records. Mice aged 5–6 mo were subjected to the analysis. Urine volume per void, voiding frequency, and total volume per day are greatly increased in $Taz^{lacZ/lacZ}$ mice (*B*) compared with $Taz^{+/lacZ}$ mice (*A*).

was well-developed in the outer cortex just beneath the capsule and contained many developing nephrons in $TAZ^{lacZ/lacZ}$ and wild-type kidneys (Fig. 5, *E–H*).

We examined the origins of the cysts using segment-specific markers. LTA, a lectin specific for the proximal tubule, stained the majority of epithelial cells lining dilated tubules and cysts in *embryonic day 18.5* $Taz^{lacZ/lacZ}$ embryos (Fig. 6, *A–D*). In contrast, no cysts were stained with DBA, a lectin specific for the collecting duct, at the same stage (Fig. 6, *E–H*). These results suggested that the cystic changes in $Taz^{lacZ/lacZ}$ kidneys primarily originated from glomeruli and proximal tubules during the maturation of induced nephrons.

Expression of Taz in developing kidneys. To correlate the renal phenotype of $Taz^{lacZ/lacZ}$ mice with *Taz* expression, we first performed in situ hybridization on wild-type embryonic kidneys. At *embryonic day 14.5*, *Taz* transcripts were diffusely expressed in both mesenchymal and epithelial cells in the developing metanephros (Fig. 7, *A* and *B*). *Taz* was also present in the ureteric bud (Fig. 7, *A* and *B*). At *embryonic day 16.5*, *Taz* was expressed in mesenchymal and epithelial cells in the nephrogenic zone and collecting ducts (Fig. 7, *C* and *D*).

In contrast to in situ hybridization, β-galactosidase activity was observed only in limited cell populations. At *embryonic day 16.5* and *day 0* postpartum, $Taz^{+/lacZ}$ kidneys exhibited sporadic *lacZ* expression in glomeruli and capillary endothelial cells that were positive for CD31 (Fig. 7, *E*, *F*, and *J–L*), indicating that *lacZ* expression may only reflect a part of the authentic *Taz* expression, possibly due to disruption of critical genomic sequences. In $Taz^{lacZ/lacZ}$ homozygous kidneys, β-galactosidase activity was detected in stromal(-like) cells, especially in the outer cortical region as well as in glomeruli and capillary endothelial cells (Fig. 7, *G–I*, *M*, and *N*). In addition, some cysts are lined by *lacZ*-positive cells in *day 0* postpartum $Taz^{lacZ/lacZ}$ kidneys (Fig. 7*O*).

Expression of cystic disease transcripts and proteins in $Taz^{lacZ/lacZ}$ *kidneys.* To find clues to the mechanism underlying the renal phenotype of $Taz^{lacZ/lacZ}$ mice, we analyzed the expression of genes involved in human PKD. No alterations in the levels of *Pkd1* and *Pkd2* mRNA and their products, polycystin-1 and polycystin-2, were observed at *embryonic day 15.5* and *18.5* by real-time RT-PCR (Fig. 8, *A* and *B*) and Western blotting (Fig. 8*D*). Also, the expression of *Pkhd1*, a gene linked to ARPKD, was not different between wild-type and $Taz^{lacZ/lacZ}$ kidneys (Fig. 8*C*). These results indicated that renal cyst formation induced by *Taz*-null mutation was not due to changes in the expression of *Pkd1*, *Pkd2*, and *Pkhd1* at the perinatal stage.

Expression of genes involved in water metabolism in $Taz^{lacZ/lacZ}$ *kidneys.* The absence of changes in the expression of cystic disease genes and concomitant diabetes insipidus-like state led us to speculate that unique pathogenetic mechanisms might

Table 2. *Defects in urinary concentration in TazlacZ/lacZ mice*

	Taz+/+	*TazlacZ/lacZ*
n	6	6
Age, wk	20–26	20–26
Body wt, g	36.8±2.1	29.4±3.1*
Water intake, ml/day	6.7±1.4	17.5±2.4*
Urine volume, ml/day	3.56±1.39	10.76±3.02*
Osmolality, mosmol/kgH_2O	2,765±646	855±131*
Urine nitrogen, mg·day^{-1}·g body wt^{-1}	4.11±0.84	3.29±1.36
Creatinine, g·day^{-1}·g body wt^{-1}	32.3±7.0	34.5±13.3
Albumin, g·day^{-1}·g body wt^{-1}	1.91±1.02	29.60±42.49
Na^+, meq·day^{-1}·g body wt^{-1}	0.011±0.004	0.011±0.002
K^+, meq·day^{-1}·g body wt^{-1}	0.034±0.007	0.035±0.009
Cl^-, meq·day^{-1}·g body wt^{-1}	0.017±0.003	0.022±0.006†

Values are means ± SD. *$P < 0.01$ and †$P < 0.05$.

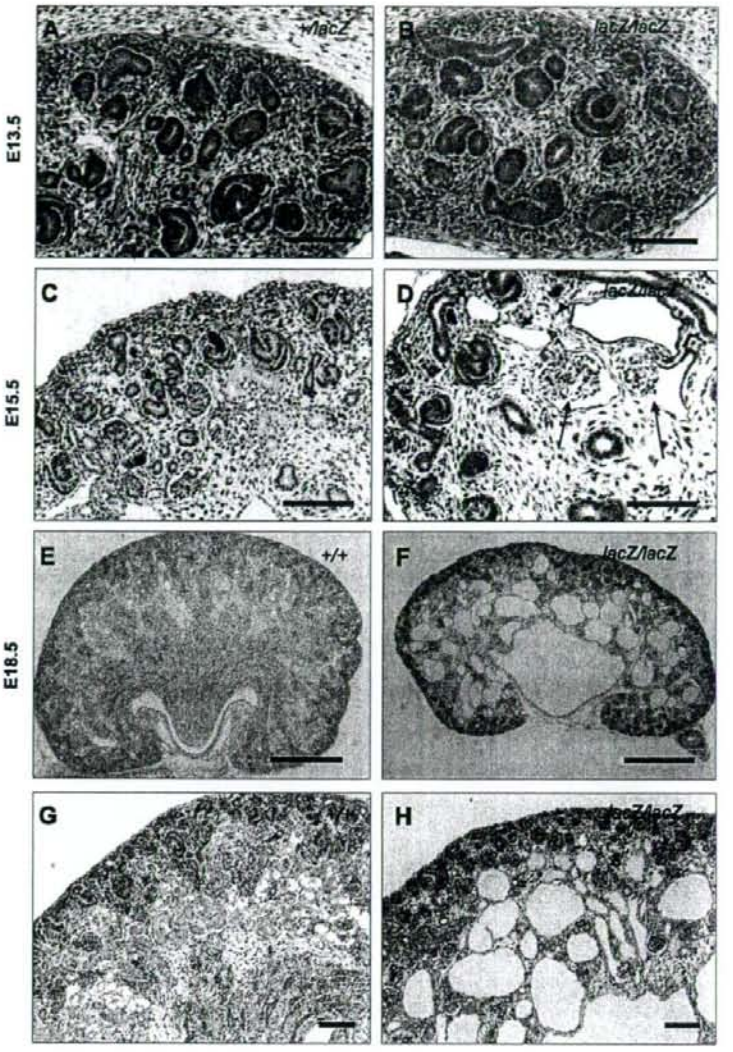

Fig. 5. Histological examination of developing kidneys in control (*A*, *C*, *E*, and *G*) and $Taz^{lacZ/lacZ}$ (*B*, *D*, *F*, and *H*) embryos. *A* and *B*: at *embryonic day 13.5*, branching of ureteric buds and formation of renal vesicles and comma- and S-shaped bodies are observed in $Taz^{lacZ/lacZ}$ (*B*) as well as wild-type and $Taz^{+/lacZ}$ (*A*) kidneys. *C* and *D*: at *embryonic day 15.5*, dilatation of Bowman's capsules (arrows) and adjacent tubules (arrowheads) are detected in $Taz^{lacZ/lacZ}$ kidneys (*D*) but not in wild-type kidneys (*C*). *E–H*: at *embryonic day 18.5*, the atrophic medulla contains multiple cysts of various sizes in $Taz^{lacZ/lacZ}$ kidneys (*F* and *H*). The pelvis is dilated and the papilla is not well formed (*F*). These changes are not observed in wild-type kidneys (*E* and *G*). The nephrogenic zone is present in the outer cortex just beneath the capsule in $Taz^{lacZ/lacZ}$ (*H*) and wild-type (*G*) kidneys. Scale bars indicate 100 μm (*A–D*, *G*, and *H*) and 500 μm (*E* and *F*).

underlie the renal phenotypes in $Taz^{lacZ/lacZ}$ kidneys. To explore the basis for disturbed water metabolism, we investigated the expression of genes and proteins that are involved in renal water transport. Although the urinary concentration defects in $Taz^{lacZ/lacZ}$ mice were resistant to exogenous vasopressin, real-time RT-PCR analysis showed that the expression of the arginine vasopressin receptor 2 gene (*Avpr2*) was largely unaffected in $Taz^{lacZ/lacZ}$ kidneys (Fig. 9*A*). The expression of aquaporin (*Aqp-1*, *-2*, and *-3*) water channels that are involved in renal water reabsorption (28) was not different among wild-type, heterozygous, and homozygous mutant kidneys (Fig. 9*B*). Immunostaining demonstrated that aquaporin-3 was localized in the basolateral membrane of epithelial cells in both $Taz^{lacZ/lacZ}$ and control $Taz^{+/lacZ}$ kidneys (Fig. 9, *C* and *D*), indicating that the polarity of aquaporin-3 localization in $Taz^{lacZ/lacZ}$ epithelial cells was intact. In $Taz^{lacZ/lacZ}$ kidneys, aquaporin-3 was expressed in many noncystic tubules and a few cysts (Fig. 9*D*), indicating an origin from the renal collecting ducts. Aquaporin-2 was also expressed similarly in collecting ducts in heterozygous and homozygous kidneys at *embryonic day 18.5* (Fig. 9, *E* and *F*). These results indicated that the renal phenotype of $Taz^{lacZ/lacZ}$ mice was not caused by changes in the expression of *Avpr2* or aquaporins.

DISCUSSION

In the present study, we demonstrate that a null mutation of *Taz* results in the formation of bilateral multicystic kidneys and

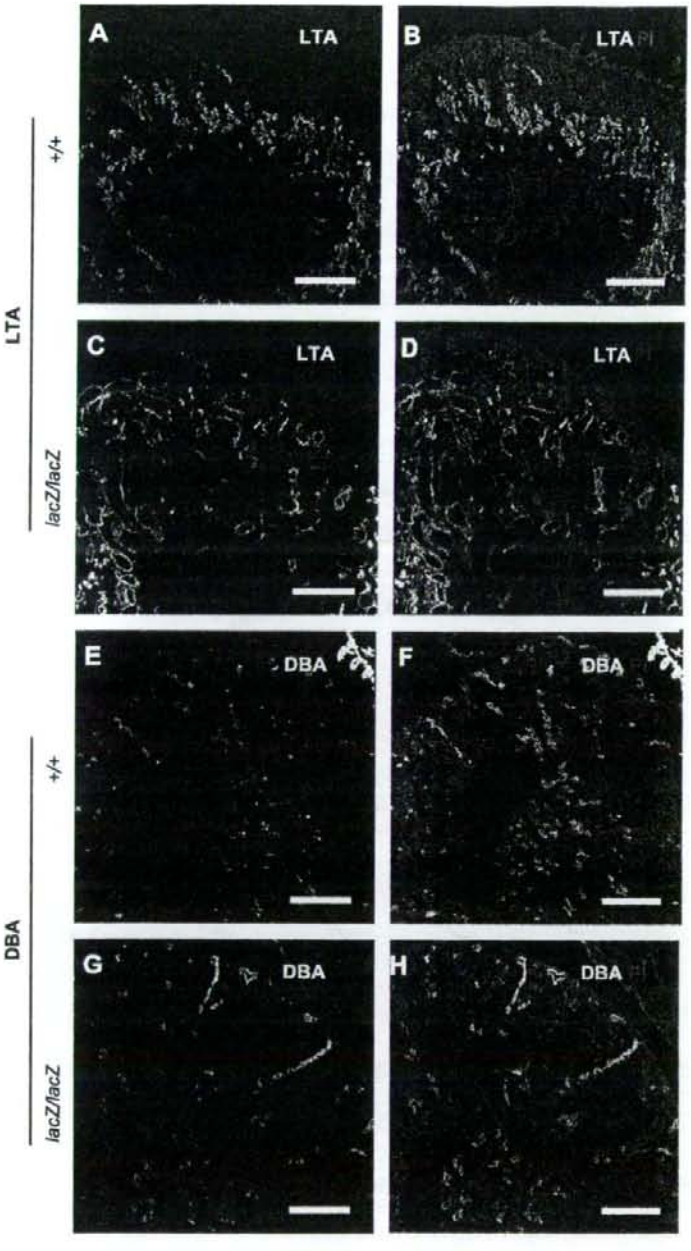

Fig. 6. Proximal tubular dilatation leading to cyst formation in $Taz^{lacZ/lacZ}$ embryos. Sections were stained with *Lotus tetragonolobus* agglutinin (LTA; *A–D*) or *Dolichos biflorus* agglutinin (DBA; *E–H*) in wild-type (*A*, *B*, *E*, and *F*) and $Taz^{lacZ/lacZ}$ (*C*, *D*, *G*, and *H*) kidneys at *embryonic day 18.5*. *B*, *D*, *F*, and *H* show costaining with propidium iodide and lectins. Epithelial cells lining dilated tubules and cysts stain positive with LTA but not with DBA in $Taz^{lacZ/lacZ}$ kidneys. Scale bars indicate 250 μm.

diffuse emphysematous changes in the lung. Renal cysts mainly originate from the glomeruli and proximal tubules around *embryonic day 15.5*, as revealed by histological features and lectin marker staining. Later, the renal changes are accompanied by pelvic dilatation and atrophy of the medulla, indicating hydronephrosis. After birth, only one-fifth of TAZ-deficient homozygotes grow to adulthood. The early mortality may be due to water and electrolyte imbalance and/or respiratory insufficiency. Surviving mutants demonstrate progressive renal changes with massive polyuria. The renal phenotype of